

Strong first order electroweak phase transition in 2HDM confronting future Z & Higgs factories

Wei Su^{*}, Anthony G. Williams^{*}, Mengchao Zhang[†]

[†]*Department of Physics and Siyuan Laboratory, Jinan University, Guangzhou 510632, P.R. China*

^{*}*ARC Centre of Excellence for Dark Matter Particle Physics, Department of Physics, University of Adelaide, South Australia 5005, Australia*

ABSTRACT: The electroweak phase transition can be made first order by extending the Standard Model (SM) Higgs sector with extra scalars. The same new physics can explain the matter-antimatter asymmetry of the universe by supplying an extra source of CP violation and sphaleron processes. In this paper we study the existence of a strong first order electroweak phase transition (SFOEWPT) in the type-I and type-II two Higgs doublet models (2HDM). We focus on how the SFOEWPT requirement constraints the spectrum of non-SM Higgs. Through a parameter space scan, we find that SFOEWPT suggests upper limits on the masses of heavy Higgs $m_{A/H/H^\pm}$, which is less than 1 TeV. High temperature expansion and Higgs vacuum uplifting is used for an analytical understanding of our results. We also study the probe ability on SFOEWPT from Higgs and Z -pole precision measurements at one-loop level at future Higgs & Z factories. And together with theoretical constraints, sizeable loop corrections require $m_A \approx m_{H^\pm} > m_H$ to meet SFOEWPT condition in Type-II 2HDM.

Contents

1	Introduction	1
2	The electroweak phase transition in 2HDMs	3
2.1	Two Higgs Doublet Models	3
2.2	Thermal effective potential	5
2.3	Numerical analysis method	6
3	Current and expected bounds	8
3.1	Theoretical constraints	8
3.2	Direct searches at LHC Run-II	9
3.3	Higgs and Z pole precision measurements	10
3.4	Flavour constraints	11
4	Study results	11
4.1	The Phase Transition of 2HDM	12
4.1.1	High Temperature Expansion	12
4.1.2	Higgs Vacuum Uplifting	13
4.2	Case1: alignment limit with fixed mass splitting	17
4.3	Case2: alignment limit with $m_A = m_{H^\pm}$	19
4.4	Case3: alignment limit with $m_H=700$ GeV	20
4.5	General results	21
5	Conclusion	25

1 Introduction

The discovery of the Higgs boson in 2012 completes the Standard Model (SM) [1, 2], yet there remain observations that cannot be explained by it. One of the most famous puzzles is the baryon asymmetry of the universe (BAU), which sees the visible matter in our universe being dominated by baryons whilst the amount of anti-baryons is negligible. Particle physics models that can successfully explain the BAU need to satisfy the three Sakharov conditions [3]. The SM was once considered as a candidate model [4–6], since baryon number conservation can be broken by an electroweak sphaleron process [4, 7, 8], the CKM matrix provides CP violation, and the electroweak phase transition can induce a departure from equilibrium if the Higgs boson is light enough. However, such an electroweak baryogenesis (EWBG) mechanism in the SM framework turns out to fail, since the CP violation present in the CKM matrix

is too small [9] and the measured Higgs mass is too heavy to trigger a strong first order electroweak phase transition (SFOEWPT) [10, 11]. Thus for a successful baryogenesis, new physics beyond the SM (BSM) is required to supply a new source of CP violation and a strong out-of-equilibrium process [12, 13]. In this work we focus on the latter issue.

In order to obtain a SFOEWPT, generally we need to extend the scalar sector of the SM. Additional parameters in the scalar sector help to change the shape of Higgs potential whilst leaving the Higgs vacuum expectation value (VEV) and the mass of Higgs same. Simple SM extensions include the addition of a $SU(2)$ singlet [14–31], an extra doublet [32–69], an extra triplet [70–73], or extra higher dimensional operators [74–79]. Consideration of the hierarchy problem leads to further solutions such as embedding the Higgs boson in a Composite Higgs model [80–82] or a supersymmetric model [83–98] to obtain a SFOEWPT. For a SFOEWPT in other models see [99–102]. In this work we study the existence of a SFOEWPT in the type-I and type-II 2HDMs [103, 104]. These models are attractive to study because the number of new parameters is relatively small. In addition, both Higgs doublets in 2HDM models are charged under $SU(2) \times U(1)$ and couple to SM fermions. This gives a greater range of observations that can probe the models relative to models that are extended by SM singlet scalars.

It is well known that, compared with other baryogenesis mechanisms, e.g. leptogenesis [105] or the Affleck–Dine mechanism [106], EWBG can be detected at the electroweak scale and part of the parameter space can be covered by current or expected collider experiments. In 2HDMs, in addition to the SM-like Higgs boson h , there are three non-SM Higgs bosons, $H/A/H^\pm$. $H/A/H^\pm$ couple to h and help to build an energy barrier between the symmetric phase and the $SU(2) \times U(1)$ broken phase when the temperature of the universe is around the electroweak scale. Then the phase transition, which is tunneling through the energy barrier, can be first order and strong enough. In our study, we will show that, in order for this strong first order phase transition to occur, the masses of H , A and H^\pm bosons should all be smaller than about 1 TeV, and generally there needs to be a relatively large mass splitting between the heavy Higgs bosons H , A and H^\pm .

H , A , and H^\pm bosons with a mass lighter than 1 TeV can be directly produced at the current LHC or future hadron colliders like the HE-LHC [107] or the SPPC [108, 109]. Channels like $A/H \rightarrow t\bar{t}/b\bar{b}/\tau\bar{\tau}$, $H^\pm \rightarrow t\bar{b}$, or $A \rightarrow HZ$ [110–113] can be used for detection or exclusion. Besides, through mixing and loop effects, the non-SM Higgs bosons also change the predicted value of the oblique parameters S , T and U , and reduce the Higgs couplings $\kappa_i = g_{hii}^{2\text{HDM}}/g_{hii}^{\text{SM}}$ relative to the SM expectation. Future e^+e^- colliders like the ILC [114], FCC-ee [115, 116] and CEPC [108, 109] will copiously produce Z and Higgs bosons, and thus those observables (especially the hZZ coupling) can be measured with unprecedented precision. In this work, we perform a global fit to obtain the parameter space of 2HDMs that simultaneously satisfies a SFOEWPT and the expected measurement precision at future Z and Higgs factories.

The structure of this paper is as follows. In Section 2 we briefly introduce our 2HDM models and calculation methods. In Section 3 we list all relevant measurements that can be

used to constrain the parameter space of the type-I and type-II 2HDMs. Section 4 starts with an analytic analysis which helps readers to understand the features of the electroweak phase transition in 2HDMs. Then we study three simplified typical cases, and present the most general scan result. We conclude this work in Section 5.

2 The electroweak phase transition in 2HDMs

2.1 Two Higgs Doublet Models

2HDMs without a \mathbb{Z}_2 symmetry generally induce dangerous flavour-violating couplings at tree level. In this work we therefore consider 2HDMs with a soft \mathbb{Z}_2 symmetry breaking. The tree-level scalar potential for a 2HDM can be written as:

$$V^0(\Phi_1, \Phi_2) = m_{11}^2 \Phi_1^\dagger \Phi_1 + m_{22}^2 \Phi_2^\dagger \Phi_2 - m_{12}^2 (\Phi_1^\dagger \Phi_2 + h.c.) + \frac{\lambda_1}{2} (\Phi_1^\dagger \Phi_1)^2 + \frac{\lambda_2}{2} (\Phi_2^\dagger \Phi_2)^2 + \lambda_3 (\Phi_1^\dagger \Phi_1) (\Phi_2^\dagger \Phi_2) + \lambda_4 (\Phi_1^\dagger \Phi_2) (\Phi_2^\dagger \Phi_1) + \frac{\lambda_5}{2} [(\Phi_1^\dagger \Phi_2)^2 + h.c.]. \quad (2.1)$$

We consider a CP-conserving case, in which all mass parameters m_{ij}^2 and quartic couplings λ_i are real. After electroweak symmetry breaking (EWSB), the two $SU(2)_L$ Higgs doublets Φ_i obtain VEVs v_i , and they can be expanded in the component real scalar fields:

$$\Phi_1 = \begin{pmatrix} \phi_1^+ \\ \frac{1}{\sqrt{2}}(v_1 + h_1 + ia_1) \end{pmatrix}, \quad \Phi_2 = \begin{pmatrix} \phi_2^+ \\ \frac{1}{\sqrt{2}}(v_2 + h_2 + ia_2) \end{pmatrix}. \quad (2.2)$$

with $v_1^2 + v_2^2 \equiv v^2 \approx (246 \text{ GeV})^2$. We further define the ratio of VEVs as $\tan \beta \equiv v_2/v_1$.

Two of the three m_{ij}^2 can be replaced by other parameters by imposing conditions that result from minimising the Higgs potential

$$m_{11}^2 = m_{12}^2 \frac{v_2}{v_1} - \frac{v_1^2}{2} \lambda_1 - \frac{v_2^2}{2} (\lambda_3 + \lambda_4 + \lambda_5) \quad (2.3)$$

$$m_{22}^2 = m_{12}^2 \frac{v_1}{v_2} - \frac{v_2^2}{2} \lambda_2 - \frac{v_1^2}{2} (\lambda_3 + \lambda_4 + \lambda_5). \quad (2.4)$$

Thus the squared mass matrices of the CP-even, CP-odd, and charged Higgs are:

$$\mathcal{M}_{\text{even}}^2 = \begin{pmatrix} m_{12}^2 \tan \beta + \lambda_1 v_1^2 & -m_{12}^2 + v_1 v_2 \lambda_{345} \\ -m_{12}^2 + v_1 v_2 \lambda_{345} & m_{12}^2 / \tan \beta + \lambda_2 v_2^2 \end{pmatrix}, \quad (2.5)$$

$$\mathcal{M}_{\text{odd}}^2 = (m_{12}^2 - v_1 v_2 \lambda_5) \begin{pmatrix} \tan \beta & -1 \\ -1 & 1/\tan \beta \end{pmatrix}, \quad (2.6)$$

$$\mathcal{M}_{\text{charged}}^2 = \left(m_{12}^2 - \frac{1}{2} v_1 v_2 (\lambda_4 + \lambda_5) \right) \begin{pmatrix} \tan \beta & -1 \\ -1 & 1/\tan \beta \end{pmatrix}. \quad (2.7)$$

Here $\lambda_{345} \equiv \lambda_3 + \lambda_4 + \lambda_5$. After diagonalization, the mass eigenstates are related to the original fields by the rotation matrices:

$$\begin{pmatrix} H \\ h \end{pmatrix} = \begin{pmatrix} \cos \alpha & \sin \alpha \\ -\sin \alpha & \cos \alpha \end{pmatrix} \begin{pmatrix} h_1 \\ h_2 \end{pmatrix}, \quad (2.8)$$

$$\begin{pmatrix} G^0 \\ A \end{pmatrix} = \begin{pmatrix} \cos \beta & \sin \beta \\ -\sin \beta & \cos \beta \end{pmatrix} \begin{pmatrix} a_1 \\ a_2 \end{pmatrix}, \quad (2.9)$$

$$\begin{pmatrix} G^\pm \\ H^\pm \end{pmatrix} = \begin{pmatrix} \cos \beta & \sin \beta \\ -\sin \beta & \cos \beta \end{pmatrix} \begin{pmatrix} \phi_1^\pm \\ \phi_2^\pm \end{pmatrix} \quad (2.10)$$

We choose our input parameters to be:

$$\cos(\beta - \alpha), \tan \beta, m_{12}^2, m_H, m_A, m_{H^\pm}. \quad (2.11)$$

The mass of the SM-like Higgs boson m_h is fixed to the current central measured value 125.09 GeV [117]. Then the λ_i can be re-expressed in terms of these input parameters. Considering the theoretical constraints, including vacuum stability, perturbativity, and unitarity, we introduce

$$\lambda v^2 \equiv m_H^2 - \frac{m_{12}^2}{\sin \beta \cos \beta}, \quad (2.12)$$

following the notation in [118]. Under the assumption of degenerate heavy Higgs masses $m_H = m_A = m_{H^\pm}$, there is no theoretical restriction on the $\tan \beta$ range when $\sqrt{\lambda v^2} = 0$.

Type-I and Type-II 2HDMs have different \mathbb{Z}_2 parity assignments, and thus the couplings between scalar and other particles have a different dependence on $\tan \beta$ and the mixing angle α . The main difference between the Type I and Type II models is the dependence of the couplings $A f \bar{f}$ and $H f \bar{f}$ on the value of $\tan \beta$. Couplings between A/H and down-type fermions are suppressed by $\frac{1}{\tan \beta}$ in the Type I model, but are enhanced by $\tan \beta$ in the Type II model. Thus the Type II model is generally more constrained by experiments than the Type I model when $\tan \beta$ is large.

Here we need to emphasize that in the 2HDM we can set the mass of the non-SM Higgs bosons $A/H/H^\pm$ to an arbitrarily high scale. This is because of the presence of $m_{11,12,22}^2$, with m_{12}^2 breaking \mathbb{Z}_2 symmetry in Eq. 2.1. As can be seen from Eq. 2.5 to Eq. 2.7, the squared masses of $A/H/H^\pm$ arise from two types of contribution. One of them involves terms of the form $\lambda_i v_j v_k$, which are bounded by perturbative unitarity and thus cannot be too large. Upper-limits on these terms are roughly given by $4\pi v^2 \approx (870 \text{ GeV})^2$. Another part of Higgs mass squares come from m_{12}^2 ($m_{11/22}^2$ are transformed through Eq. (2.3) and Eq. (2.4)), and these terms can in principle be set to any value without violating theoretical requirements. This makes the search for evidence of 2HDMs an endless game: you can never completely falsify a New Physics model containing hypothetical particles which have no upper limits on their mass.

However, in the following part of this work we will show that the requirement of a SFOEWPT imposes upper limits on the masses of the $A/H/H^\pm$ bosons, making it possible to fully verify or falsify the idea of EWBG in 2HDMs in the near future.

2.2 Thermal effective potential

To study the phase transition in the early universe, we need to study the dependence of the free energy density on the order parameter. In our case, the free energy density is the thermal effective potential, and the order parameter is the homogeneous scalar VEV [119]. The thermal effective potential $V(\phi_1, \phi_2, T)$ at temperature T is composed of four parts:

$$V(\phi_1, \phi_2, T) = V^0(\phi_1, \phi_2) + V^{\text{CW}}(\phi_1, \phi_2) + V^{\text{CT}}(\phi_1, \phi_2) + V^{\text{T}}(\phi_1, \phi_2, T). \quad (2.13)$$

Here V^0 is the tree-level potential of our model, V^{CW} is one-loop Coleman-Weinberg potential, V^{CT} is the counter term, and V^{T} is the thermal correction.

The tree-level potential $V^0(\phi_1, \phi_2)$ is obtained by replacing the field operators $\Phi_1(x)$ and $\Phi_2(x)$ in $V^0(\Phi_1, \Phi_2)$ with the homogeneous field values $\frac{1}{\sqrt{2}}(0, \phi_1)^T$ and $\frac{1}{\sqrt{2}}(0, \phi_2)^T$:

$$V^0(\phi_1, \phi_2) = \frac{1}{2}m_{11}^2\phi_1^2 + \frac{1}{2}m_{22}^2\phi_2^2 - m_{12}^2\phi_1\phi_2 + \frac{1}{8}\lambda_1\phi_1^4 + \frac{1}{8}\lambda_2\phi_2^4 + \frac{1}{4}\lambda_{345}\phi_1^2\phi_2^2. \quad (2.14)$$

The one-loop Coleman-Weinberg potential $V^{\text{CW}}(\phi_1, \phi_2)$ is given in the $\overline{\text{MS}}$ renormalization scheme by [120]:

$$V^{\text{CW}}(\phi_1, \phi_2) = \frac{1}{64\pi^2} \sum_i n_i m_i^4(\phi_1, \phi_2) \left[\ln \frac{m_i^2(\phi_1, \phi_2)}{\mu^2} - c_i \right], \quad (2.15)$$

with the index i running over all massive particles. n_i is the degrees of freedom of particle i multiplied by $(-1)^{2s}$ (s is the spin of particle i), which is -12, -4, 6, 3, 2, 1, 2 and 1 for quarks, leptons, W^\pm , Z , H^\pm , G^0 , G^\pm , and neutral scalars, respectively. c_i is $\frac{5}{6}$ for gauge bosons, and $\frac{3}{2}$ for other particles. $m_i^2(\phi_1, \phi_2)$ is the mass square of particle i with v_1 and v_2 in its expression being replaced by scalar field value ϕ_1 and ϕ_2 . The renormalization scale μ is set to the zero temperature VEV v .

In Eq. 2.11 we choose the scalar masses, mixing angle, and VEV ratio as our input parameters. These parameters are considered as physical parameters. It means that the VEVs are determined by the position of the minimum of the scalar potential, and squared masses are given by the second order partial derivatives of the scalar potential with respect to the scalar fields at the position of the minimum. Adding the Coleman-Weinberg correction will shift both the position of the minimum and the second order partial derivatives of the tree-level potential.

Thus, in order to offset the modification, counter terms $V^{\text{CT}}(\Phi_1, \Phi_2)$ need to be added to the Lagrangian. For a CP-conserving 2HDM, $V^{\text{CT}}(\Phi_1, \Phi_2)$ can be expressed as [52]:

$$\begin{aligned} V^{\text{CT}}(\Phi_1, \Phi_2) = & \delta m_{11}^2 \Phi_1^\dagger \Phi_1 + \delta m_{22}^2 \Phi_2^\dagger \Phi_2 - \delta m_{12}^2 \left(\Phi_1^\dagger \Phi_2 + h.c. \right) + \frac{\delta \lambda_1}{2} \left(\Phi_1^\dagger \Phi_1 \right)^2 + \frac{\delta \lambda_2}{2} \left(\Phi_2^\dagger \Phi_2 \right)^2 \\ & + \delta \lambda_3 \left(\Phi_1^\dagger \Phi_1 \right) \left(\Phi_2^\dagger \Phi_2 \right) + \delta \lambda_4 \left(\Phi_1^\dagger \Phi_2 \right) \left(\Phi_2^\dagger \Phi_1 \right) + \frac{\delta \lambda_5}{2} \left[\left(\Phi_1^\dagger \Phi_2 \right)^2 + h.c. \right] \\ & + \delta t_1 \phi_1 + \delta t_2 \phi_2. \end{aligned} \quad (2.16)$$

Coefficients of counter terms, those δs , need to be fixed by “on-shell” conditions:

$$\begin{aligned}\partial_{\psi_i} (V^{\text{CT}}(\Phi_1, \Phi_2) + V^{\text{CW}}(\Phi_1, \Phi_2)) &= 0 \\ \partial_{\psi_i} \partial_{\psi_j} (V^{\text{CT}}(\Phi_1, \Phi_2) + V^{\text{CW}}(\Phi_1, \Phi_2)) &= 0,\end{aligned}\tag{2.17}$$

with ψ_i denoting all of the component scalar fields of Φ_1 and Φ_2 . These conditions are evaluated at the minimum of the scalar potential at zero temperature, where $\Phi_1 = \frac{1}{\sqrt{2}}(0, v_1)^T$ and $\Phi_2 = \frac{1}{\sqrt{2}}(0, v_2)^T$ ¹. After adding these counter terms, our input parameters can be treated as physical parameters which are directly connected to observables.

The thermal correction with ring resummation included is [121, 122]:

$$\begin{aligned}V^T(\phi_1, \phi_2, T) &= \frac{T^4}{2\pi^2} \sum_i n_i J_B \left(\frac{m_i^2(\phi_1, \phi_2)}{T^2} \right) + \frac{T^4}{2\pi^2} \sum_j n_j J_F \left(\frac{m_j^2(\phi_1, \phi_2)}{T^2} \right) \\ &\quad - \frac{T^4}{12\pi} \sum_k n_k \left[\left(\frac{\tilde{m}_k^2(\phi_1, \phi_2, T)}{T^2} \right)^{3/2} - \left(\frac{m_k^2(\phi_1, \phi_2)}{T^2} \right)^{3/2} \right].\end{aligned}\tag{2.18}$$

Here, the index i denotes all gauge bosons and scalars, j denotes leptons and quarks, and k denotes scalars and the longitudinal component of gauge bosons. The functions $J_{B,F}$ are two integrals which come from the scalar and fermion thermal corrections respectively:

$$J_B(x) = \int_0^\infty dk \, k^2 \ln \left[1 - \exp(-\sqrt{k^2 + x}) \right],\tag{2.19}$$

$$J_F(x) = \int_0^\infty dk \, k^2 \ln \left[1 + \exp(-\sqrt{k^2 + x}) \right].\tag{2.20}$$

The second line in 2.19 comes from ring resummation, which is used to avoid the infrared divergence that occurs when the scalar mass is much smaller than the temperature. $\tilde{m}_k^2(\phi_1, \phi_2, T)$ is the thermal Debye mass, an expression for which can be found in the literature [52, 122].

2.3 Numerical analysis method

An electroweak phase transition is considered to be strong enough only if the net baryon number generated around the bubble wall is not significantly washed out by the sphaleron process inside the bubble. This condition can be converted to the requirement on the value of “wash out” parameter [123]:

$$\xi_c \equiv \frac{v_c}{T_c} > 0.9\tag{2.21}$$

Here T_c is the critical temperature where a second minimum of $V(\phi_1, \phi_2, T)$ that breaks $SU(2) \times U(1)$ appears, and $v_c \equiv \sqrt{v_1^2(T_c) + v_2^2(T_c)}$ reflects the scale of electroweak symmetry breaking. Here $v_1(T_c)$ and $v_2(T_c)$ are the scalar field values which minimize $V(\phi_1, \phi_2, T_c)$.

¹Second order derivatives of V^{CW} suffer from an infrared divergence originating from the massless Goldstone boson when $T = 0$. This problem can be solved by introducing an IR cut-off mass [50].

The calculation of ξ_c suffers from theoretical uncertainties. The first problem is that the ξ_c induced by $V(\phi_1, \phi_2, T)$ is not gauge independent by itself [124–126]. Missing higher-order quantum corrections also induce a theoretical uncertainty [127]. For a concrete model, one can use lattice simulations to obtain a reliable value of ξ_c [63], but such a non-perturbative calculation is very computationally expensive. Being aware of the theoretical uncertainty in the calculation of ξ_c , in this work we relax the criterion of a SFOEWPT to $\xi_c \equiv \frac{v_c}{T_c} > 0.9$. On the other hand, for a first order phase transition to really happen in the universe, the bubble nucleation rate should be larger than the Hubble expansion rate at the nucleation temperature [33, 128]. This requirement can be considered as a further constraint on the 2HDM parameter space. For a conservative estimate, in this work we will not consider a requirement on the bubble nucleation rate.

Analytically, T_c and v_c can be obtained by solving the following equations:

$$V(0, 0, T_c) = V(v_1(T_c), v_2(T_c), T_c), \quad (2.22)$$

$$\left. \frac{\partial}{\partial \phi_1} V(\phi_i, \phi_2, T_c) \right|_{\phi_1=v_1(T_c), \phi_2=v_2(T_c)} = 0 \quad (i = 1, 2), \quad (2.23)$$

$$\left. \frac{\partial}{\partial \phi_1} V(\phi_i, \phi_2, T_c) \right|_{\phi_1=0, \phi_2=0} = 0 \quad (i = 1, 2). \quad (2.24)$$

To make $(0, 0)$ and $(v_1(T_c), v_2(T_c))$ as local minimum points of $V(\phi_i, \phi_2, T_c)$, Hessian matrix of $V(\phi_i, \phi_2, T_c)$ at $(0, 0)$ and $(v_1(T_c), v_2(T_c))$ also need to be positive definite. However, due to the complicated form of $V(\phi_1, \phi_2, T)$, solving these equations analytically is quite difficult. Instead, one can search for the critical temperature using a numerical method. There are already public packages which can be used for numerical thermal phase transition analysis, such as **CosmoTransitions** [129], **BSMPT** [61], and **PhaseTracer** [130]. We choose **BSMPT** for our numerical analysis, since the 2HDM has been implemented in **BSMPT** as a benchmark model, and **BSMPT** is written in **C++** which helps to save numerical calculation time. In **BSMPT**, the search for T_c is started from a high temperature (the default value is 300 GeV), where the minimum position of $V(\phi_1, \phi_2, T)$ is $(0, 0)$. Then **BSMPT** traces the minimum position of $V(\phi_1, \phi_2, T)$ with decreasing temperature. If **BSMPT** detects a minimum position jumping $(0, 0) \Rightarrow (v_1(T'), v_2(T'))$ at a certain temperature T' , the search stops and the output T' is the desired critical temperature T_c .

The full thermal phase transition history of the 2HDM could be complicated [59]. Multiple phase transition processes are possible. For baryogenesis, however, only the phase transition that transfers $(0, 0) \Rightarrow (v_1(T), v_2(T))$ is relevant. This is because a successful baryogenesis requires the sphaleron rate to be very fast outside the bubble wall, i.e. $\Gamma_{\text{Sph}} \sim (\alpha_W T)^4$. While in the electroweak symmetry breaking phase, the sphaleron rate will be strongly suppressed as $\Gamma_{\text{Sph}} \propto \exp(-E_{\text{Sph}}(T_c)/T_c)$. Here the sphaleron energy $E_{\text{Sph}}(T_c) \sim 10\text{TeV} \times \frac{v_c}{v}$. Thus another phase transition $(v_1(T''), v_2(T'')) \Rightarrow (w_1(T''), w_2(T''))$ has nothing to do with baryogenesis, because the sphaleron rate outside the bubble will be too low to generate baryon number. We will therefore not take this kind of phase transition into account in this work.

3 Current and expected bounds

2HDMs are constrained by various theoretical considerations and experimental measurements, such as vacuum stability, perturbativity and unitarity, as well as heavy flavor observations [131], electroweak precision measurements, and LHC Higgs measurements and non-SM Higgs searches [132]. We briefly summarize below the constraints we adopt in the following sections.

3.1 Theoretical constraints

- **Vacuum stability**

In order to make the vacuum stable, the scalar potential should be bounded from below [133–136]:

$$\lambda_1 > 0, \lambda_2 > 0, \lambda_3 > -\sqrt{\lambda_1 \lambda_2}, \lambda_3 + \lambda_4 - |\lambda_5| > -\sqrt{\lambda_1 \lambda_2} \quad (3.1)$$

- **Perturbativity and unitarity**

We adopt a general perturbativity condition of $|\lambda_i| \leq 4\pi$, and for the unitarity bound [137–141]:

$$\left| 3(\lambda_1 + \lambda_2) \pm \sqrt{9(\lambda_1 - \lambda_2)^2 + 4(2\lambda_3 + \lambda_4)^2} \right| < 16\pi, \quad (3.2)$$

$$\left| (\lambda_1 + \lambda_2) \pm \sqrt{(\lambda_1 - \lambda_2)^2 + 4\lambda_4^2} \right| < 16\pi, \quad (3.3)$$

$$\left| (\lambda_1 + \lambda_2) \pm \sqrt{(\lambda_1 - \lambda_2)^2 + 4\lambda_5^2} \right| < 16\pi, \quad (3.4)$$

$$|\lambda_3 + 2\lambda_4 \pm 3\lambda_5| < 8\pi, \quad |\lambda_3 \pm \lambda_4| < 8\pi, \quad |\lambda_3 \pm \lambda_5| < 8\pi \quad (3.5)$$

To provide some general insights into the impact of these theoretical constraints, we show in Fig. 1 the allowed regions in the $m_H - \Delta m$ (left), $m_H - \tan \beta$ (middle), and $\lambda v^2 - \tan \beta$ (right) planes, for various fixed values of the other parameters. In the left panel, we take $\tan \beta = 3, \cos(\beta - \alpha) = 0$, fixing $m_A = m_{H^\pm}$. Here $\sqrt{\lambda v^2} = 0, 150, 300, 220, 230$ GeV are represented by the red, blue, green, purple, and orange lines, and the region under the lines is allowed by the theoretical constraints. Generally, a larger heavy Higgs mass m_H corresponds to a smaller allowed mass splitting Δm for any specific $\sqrt{\lambda v^2}$. The allowed Δm also gets smaller when $\sqrt{\lambda v^2}$ gets larger, and here there is no region left for $\sqrt{\lambda v^2} > 232$ GeV.

In the middle panel with $\sqrt{\lambda v^2} = 0$ GeV, we explore the effect of the parameter $\cos(\beta - \alpha)$. Here, based on the allowed $|\cos(\beta - \alpha)|$ at the current LHC Run-II [142], we take $\cos(\beta - \alpha) = \pm 0.005$ (dashed lines), and $\cos(\beta - \alpha) = \pm 0.02$ (solid lines) and show the allowed region, which is to the left of the corresponding lines. We fix the mass splitting $\Delta m = m_{A/H^\pm} - m_H = 200$ GeV. Under $\cos(\beta - \alpha) = 0$, $m_H < 820$ GeV is allowed, independently of $\tan \beta$. If $\cos(\beta - \alpha) \neq 0$, such as the 0.005 region shown by the dashed lines, the allowed regions are

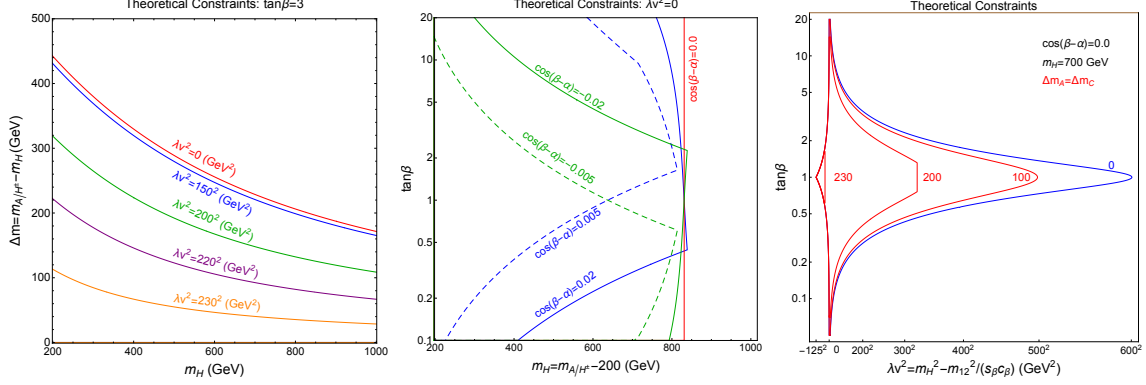


Figure 1. The impact of theoretical constraints in the $m_H - \Delta m$ (left), $m_H - \tan\beta$ (middle), $\lambda v^2 - \tan\beta$ (right) planes. In the left panel, the allowed region is under the lines with $\tan\beta = 3, \cos(\beta - \alpha) = 0$. In the middle panel, $\sqrt{\lambda v^2} = 0$ GeV, and the allowed region is to the left of the corresponding lines. In the right panel, m_H is fixed at 700 GeV, and the allowed region is inside of the boundary line. See text for full details.

reduced. As discussed in [118], the allowed regions for opposite-sign $\cos(\beta - \alpha)$ are symmetric around the line $\tan\beta = 1$.

In the right panel, m_H is fixed at 700 GeV, and $\Delta m = m_{A/H^\pm} - m_H = 0, 100, 200$ and 230 are shown. The allowed region is inside of the boundary line. Larger Δm leads to a smaller allowed λv^2 range, and $\Delta m > 230$ GeV is no longer allowed. For $\sqrt{\lambda v^2} = 0$, there is no restriction on $\tan\beta$.

3.2 Direct searches at LHC Run-II

We take into account the latest heavy Higgs searches at LHC Run-II, including $A/H \rightarrow \mu\mu$ [143, 144], $A/H \rightarrow b\bar{b}$ [145, 146], $A/H \rightarrow \tau\tau$ [147–149], $A/H \rightarrow \gamma\gamma$ [150–154], $A/H \rightarrow t\bar{t}$ [155], $H \rightarrow ZZ$ [156, 157], $H \rightarrow WW$ [158, 159], $A \rightarrow hZ \rightarrow b\bar{b}l\bar{l}$ [160–163], $A \rightarrow hZ \rightarrow \tau\tau\ell\bar{\ell}$ [162, 164, 165], $H \rightarrow hh$ [166–169], and $A/H \rightarrow HZ/AZ$ [170, 171]. To investigate the impact on the 2HDM parameter space of the published null results in these searches, we take the cross section times branching fraction limits, $\sigma \times \text{BR}$, from the LHC studies and reinterpret them for our 2HDM model points using the **SusHi** package [172] to calculate the production cross-section at NNLO level, and the **2HDMC** [173] code for Higgs decay branching fractions at tree level.

As a first example, taking the benchmark point $\cos(\beta - \alpha) = 0$, $m_{12}^2 = m_H^2 \cos\beta \sin\beta$ and $m_A = m_{H^\pm} = m_H + 200$ GeV, we show the current collider limits in the $m_H - \tan\beta$ plane in Fig. 2, for both the Type I and Type II models. The various channels include $H/A \rightarrow b\bar{b}$ (red), $H/A \rightarrow \tau\tau$ (dotted orange), $H/A \rightarrow \mu\mu$ (dot-dashed cyan), $H/A \rightarrow \gamma\gamma$ (dashed brown), $H/A \rightarrow t\bar{t}$ (dot-dashed magenta) and $4t$ production (dashed purple), as well as the exotic decay channel $A \rightarrow HZ$ (blue). Other decays such as $A \rightarrow Zh$ and $H \rightarrow hh$ will only contribute if $\cos(\beta - \alpha)$ deviates from zero at tree level [174].

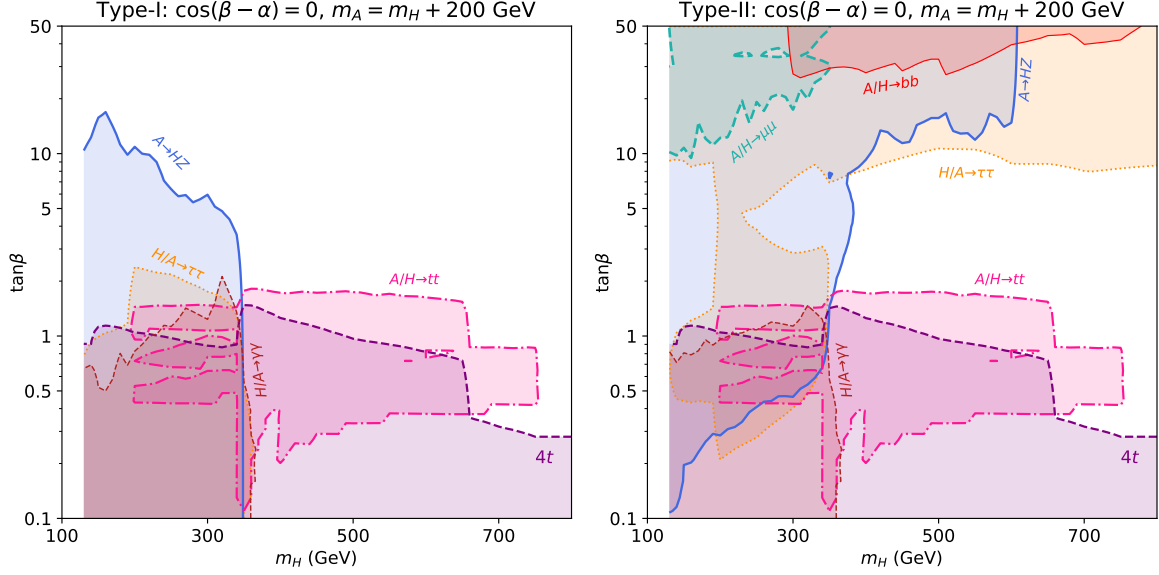


Figure 2. Direct search constraints for the heavy Higgs mass spectrum $m_A = m_{H^\pm} = m_H + 200$ GeV. We show the 95% C.L. exclusion region in the $m_H - \tan \beta$ plane for the Type-I 2HDM (left) and Type-II 2HDM (right) with $\cos(\beta - \alpha) = 0$. The various heavy Higgs decays include i) the conventional search results on $H/A \rightarrow bb$ (red), $H/A \rightarrow \tau\tau$ (dotted orange), $H/A \rightarrow \mu\mu$ (dot-dashed cyan), $H/A \rightarrow \gamma\gamma$ (dashed brown), $H/A \rightarrow tt$ (dot-dashed magenta) and $4t$ production (dashed purple), and ii) exotic decay channels $A \rightarrow HZ$ (blue). Other considered decays such as $A \rightarrow Zh$, $H \rightarrow hh$ are not relevant since their couplings are proportional to $\cos(\beta - \alpha)$.

For the Type-I model (left panel of Fig. 2), the exotic decay $A \rightarrow HZ$ channel covers $m_H < 2m_t$, $\tan \beta < 5$ totally, and can reach to $\tan \beta = 10$. Top quarks searches, $4t + A/H \rightarrow tt$, cover $m_H < 800$ GeV for $\tan \beta < 0.3$, and $m_H < 650$ GeV for $\tan \beta < 1.1$. $A/H \rightarrow \tau\tau, \gamma\gamma$ then exclude the region $m < 350$ GeV, $\tan \beta < 1$. Generally because of the $\cot \beta$ -enhanced Yukawa coupling in Type-I model, only the small $\tan \beta$ region can be explored[132]. In the Type-II 2HDM (right panel), the top quark and $H/A \rightarrow \gamma\gamma$ constraints are similar to those for the Type-I model, while the fermionic decays $A/H \rightarrow bb, \tau\tau, \mu\mu$ could exclude m_H to 800 GeV when $\tan \beta > 10$ generally. Since the Hbb , and $H\tau\tau$ couplings are $\tan \beta$ -enhanced, the $A \rightarrow HZ$ decay contributes a lot at medium and large $\tan \beta$ regions, $\tan \beta > 0.5$, $m_H < 2m_t$ and $\tan \beta > 15$, $m_H < 600$ GeV. Thus $m_H < 2m_t$ is totally excluded by all channels together in Type-II model, and only $1.5 < \tan \beta < 10$ is allowed for $m_H < 650$ GeV, which is important for our later study of the electroweak phase transition.

3.3 Higgs and Z pole precision measurements

The SM has been tested with high precision via observables measured at the Z -pole from LEP-I [175] and the LHC [176]. Future lepton colliders will further improve the precision of measurements in the Higgs sector, and we therefore include hypothetical future lepton collider results in our study. In Ref. [177], it was shown that the precision reached by several

future e^+e^- machines, including the CEPC program with an integrated luminosity of 5.6 ab^{-1} [108, 109], the FCC-ee program with 5 ab^{-1} of integrated luminosity [115, 116], and the ILC with various center-of-mass energies [114], is similar. Thus, following the approach adopted in Ref. [177, 178], we will explore the CEPC proposals in detail.

In our analyses, we take the S, T, U data at 95% Confidence Level (C.L.) from Table 2 of Ref. [177], and the Higgs precision measurements from Table 3 in the same reference. We use a χ^2 profile-likelihood fit,

$$\chi^2 = \sum_{ij}^Z (X_i - \hat{X}_i)(\sigma^2_{ij})^{-1}(X_j - \hat{X}_j) + \sum_i^H \frac{(\mu_i^{\text{2HDM}} - \mu_i^{\text{obs}})^2}{\sigma_{\mu_i}^2}, \quad (3.6)$$

with $X_i = (\Delta S, \Delta T, \Delta U)_{\text{2HDM}}$ being the 2HDM predicted values, and $\hat{X}_i = (\Delta S, \Delta T, \Delta U)$ being the current best-fit central value for current measurements, and 0 for future measurements at the first term for Z sector. The σ_{ij} are the error matrix, $\sigma_{ij}^2 \equiv \sigma_i \rho_{ij} \sigma_j$ with σ_i and correlation matrix ρ_{ij} given in [177]. For the second term about Higgs sector, Higgs precision measurements are used to perform global fit with $\mu_i^{\text{2HDM}} = (\sigma_i \times \text{Br}_i)^{\text{2HDM}} / (\sigma_i \times \text{Br}_i)^{\text{SM}}$ is the signal strength for various Higgs search channels, σ_{μ_i} is the estimated error for each process. The studies [177, 178] show that one-loop level electroweak corrections to SM Higgs couplings have probe ability to heavy Higgs with Higgs precision measurements, and thus our study of

For future colliders, the various μ_i^{obs} are set to be unity in the current analyses, assuming no deviations from the SM observables.

In the following analyses, the overall χ^2 is calculated, and use to determine the allowed parameter region at the 95% C.L. For the one-, and two-parameter fits, the corresponding $\Delta\chi^2 = \chi^2 - \chi_{\min}^2$ values at the 95% C.L. are 3.84, and 5.99 respectively.

3.4 Flavour constraints

The charged Higgs H^\pm boson couples to up and down type fermions, and thus observations from flavor physics put strong bounds on its mass and couplings [179]. Among various flavor observations, measurements related to B physics provide the most stringent limits on $\tan\beta$ and m_{H^\pm} . For example, $m_{H^\pm} < 580 \text{ GeV}$ in the Type-II 2HDM has been excluded by the measurement of $BR(B \rightarrow X_s \gamma)$ [180]. ΔM_{B_s} and $BR(B_s \rightarrow \mu^+ \mu^-)$ further exclude $m_{H^\pm} < 1 \text{ TeV}$ in the Type-II 2HDM when $\tan\beta < 0.7$. The region with $\tan\beta < 1$ and $m_{H^\pm} < 1 \text{ TeV}$ in the Type-I 2HDM has been excluded by $B \rightarrow X_s \gamma$ [180]. In our study, we take these constraints into account.

4 Study results

Based on the diverse constraints above, in this section we will discuss their effects on the SFOEWPT in Type-I and Type-II 2HDMs.

4.1 The Phase Transition of 2HDM

To get a better understanding of the electroweak phase transition in 2HDMs, we will first discuss it in the context of some approximate or limiting cases, focusing on the relationship between the phase transition and the Higgs vacuum uplifting. Then we will consider several benchmark cases, varying one or two parameters to dig into the effects of constraints as well as features of the Higgs potential. Our general results will follow these specific cases.

4.1.1 High Temperature Expansion

Due to the complicated form of the thermal effective potential [Eq. \(2.13\)](#) and its intricate thermal evolution history, it is difficult to tell whether a specific point can successfully trigger a SFOEWPT in the early universe through a simple formula or argument. To simplify the analysis of the phase transition, people generally use a high temperature expansion, limited to the leading terms of the thermal correction functions J_B and J_F . Then the thermal effective potential can be simplified to a polynomial function of the Higgs field value:

$$V(\phi_h, T) \approx (DT^2 - \mu^2)\phi_h^2 - ET\phi_h^3 + \frac{\tilde{\lambda}}{4}\phi_h^4 \quad (4.1)$$

Here $\phi_h \equiv \cos\beta\phi_1 + \sin\beta\phi_2$ is the scalar field that breaks the $SU(2) \times U(1)$ symmetry at zero temperature. Due to the simple form of [Eq. 4.1](#), we can use the minimization condition and $V(0, T_c) = V(v_c, T_c)$ to directly calculate the wash-out parameter:

$$\xi_c \equiv \frac{v_c}{T_c} \approx \frac{2E}{\tilde{\lambda}} \quad (4.2)$$

At tree-level, the coefficients μ^2 and $\tilde{\lambda}$ in [Eq. \(4.1\)](#) are:

$$\mu^2 = \frac{1}{4}m_h^2, \quad \tilde{\lambda} = \frac{m_h^2}{2v^2} \quad (4.3)$$

The coefficients D and E are induced from the leading thermal corrections:

$$\frac{T^4}{2\pi^2}J_B\left(\frac{m^2(\phi_h)}{T^2}\right) \approx -\frac{\pi^2 T^4}{90} + \frac{1}{24}T^2 m^2(\phi_h) - \frac{1}{12\pi}T(m^2(\phi_h))^{3/2} + \dots \quad (4.4)$$

$$\frac{T^4}{2\pi^2}J_F\left(\frac{m^2(\phi_h)}{T^2}\right) \approx +\frac{7}{8}\frac{\pi^2 T^4}{90} - \frac{1}{48}T^2 m^2(\phi_h) + \dots \quad (4.5)$$

Here $m^2(\phi_h)$ is the mass square of a massive particle with v^2 in it being replaced by ϕ_h^2 (For example, $m_W^2(\phi_h) = \frac{m_W^2}{v^2}\phi_h^2$). Considering the most massive particles in the 2HDM, D and E can be expressed as:

$$D = \frac{1}{24} \left[6\frac{m_W^2}{v^2} + 3\frac{m_Z^2}{v^2} + \frac{m_h^2}{v^2} + 6\frac{m_t^2}{v^2} + \frac{m_H^2 - M^2}{v^2} + \frac{m_A^2 - M^2}{v^2} + 2\frac{m_{H^\pm}^2 - M^2}{v^2} \right] \quad (4.6)$$

$$E = \frac{1}{12\pi} \left[6\frac{m_W^3}{v^3} + 3\frac{m_Z^3}{v^3} + \frac{m_h^3}{v^3} \right] + E_{(H/A/H^\pm)}$$

In the expression for E , the term $E_{(H/A/H^\pm)}$ denotes the contributions from the non-SM Higgs bosons. We cannot explicitly write out the expression for $E_{(H/A/H^\pm)}$ because, as we said in Section 2.1, the mass of the $H/A/H^\pm$ bosons come from two sources. Schematically, the ϕ_h -dependent non-SM Higgs squared masses can be expressed as:

$$m_\alpha^2(\phi_h) = M^2 + \lambda_\alpha \phi_h^2 \quad (4.7)$$

Here $M^2 = \frac{m_{12}^2}{\sin\beta \cos\beta}$ is the scale at which the \mathbb{Z}_2 symmetry is broken. α can be A , H , or H^\pm , and λ_α is a linear combination of the $\lambda_i (i = 1, 2, 3, 4, 5)$ parameters. In the alignment limit $\cos(\beta - \alpha) = 0$, the expressions for λ_α are:

$$\lambda_H = (\lambda_1 + \lambda_2 - 2\lambda_{345})(\sin^2\beta \cos^2\beta) , \quad (4.8)$$

$$\lambda_A = -\lambda_5 , \quad (4.9)$$

$$\lambda_{H^\pm} = -\frac{1}{2}(\lambda_4 + \lambda_5) \quad (4.10)$$

So the non-SM Higgs bosons provide a term in $V(\phi_h, T)$ which is not exactly proportional to ϕ_h^3 :

$$-\frac{1}{12\pi}T(m_\alpha^2(\phi_h))^{3/2} = -\frac{1}{12\pi}T(M^2 + \lambda_\alpha \phi_h^2)^{3/2} \quad (4.11)$$

We can simplify the above expression in two limiting cases:

$$-\frac{1}{12\pi}T(M^2 + \lambda_\alpha \phi_h^2)^{3/2} \approx \begin{cases} -\frac{T}{12\pi}\lambda_\alpha^{3/2}\phi_h^3, & M^2 \ll \lambda_\alpha \phi_h^2 \\ -\frac{T}{12\pi}M^3 \left(1 + \frac{3}{2}\frac{\lambda_\alpha \phi_h^2}{M^2}\right), & M^2 \gg \lambda_\alpha \phi_h^2 \end{cases} \quad (4.12)$$

And so in these two limiting cases:

$$E_{(\alpha)} \approx \begin{cases} \frac{1}{12\pi}\lambda_\alpha^{3/2} = \frac{1}{12\pi}\frac{m_\alpha^3}{v^3}, & M^2 \ll \lambda_\alpha \phi_h^2 \\ 0, & M^2 \gg \lambda_\alpha \phi_h^2 \end{cases} \quad (4.13)$$

The above expression needs to be multiplied by 2 if α is H^\pm .

Although expression 4.13 is obtained in a limiting case, it helps us to understand which of the input parameters are particularly relevant for a SPOEWPT. When the non-SM Higgs masses are dominated by M^2 , the spectrum tends to be degenerate, and the phase transition strength tends to be reduced as the non-SM Higgs boson masses increase. When the non-SM Higgs masses are dominated by $\lambda_\alpha v^2$, the spectrum tends to be split, and the phase transition strength tends to be increased as the non-SM Higgs boson masses increase.

4.1.2 Higgs Vacuum Uplifting

Another method that can help us to understand which parameters are important for SFOEWPT, is to calculate the depth of the zero temperature Higgs potential [55]. For a shallow Higgs potential, it is easier to develop an energy barrier between the symmetric phase and the

broken phase than for a deep Higgs potential, when the temperature is high. Thus generally speaking, there is an inverse relation between the phase transition strength and the depth of the vacuum energy. We follow the notation at Ref. [55] and define the SM vacuum energy density as $\mathcal{F}_0^{\text{SM}}$. The value of $\mathcal{F}_0^{\text{SM}}$ is about $-1.25 \times 10^8 \text{ GeV}^4$. The vacuum energy density of the 2HDM is denoted by \mathcal{F}_0 . We can further define a dimensionless parameter:

$$\Delta\mathcal{F}_0/|\mathcal{F}_0^{\text{SM}}| \equiv \frac{\mathcal{F}_0 - \mathcal{F}_0^{\text{SM}}}{|\mathcal{F}_0^{\text{SM}}|} \quad (4.14)$$

$\Delta\mathcal{F}_0/|\mathcal{F}_0^{\text{SM}}| > 0$ means that the 2HDM vacuum energy is uplifted from the SM value, whilst $\Delta\mathcal{F}_0/|\mathcal{F}_0^{\text{SM}}|$ cannot exceed 1, otherwise the zero temperature vacuum will be unstable. The numerical results in [55] show a positive correlation between ξ_c and the parameter $\Delta\mathcal{F}_0/|\mathcal{F}_0^{\text{SM}}|$. However, we find that the relationship is only valid for $m_H \leq 500 \text{ GeV}$, the range Ref [55] explored, and the parameters may become negatively-correlated for large m_H . To illustrate this, here we refine their analysis by considering a benchmark case:

$$\begin{aligned} \tan\beta = 3.0, \quad \cos(\beta - \alpha) = 0, \quad m_H \in (200, 1000) \text{ GeV}, \\ \sqrt{\lambda v^2} = 0, \quad \Delta m = m_{A/H^\pm} - m_H = 200 \text{ GeV}. \end{aligned} \quad (4.15)$$

All parameters are fixed except m_H , and $\lambda v^2 = m_H^2 - \frac{m_{12}^2}{\sin\beta\cos\beta} = 0$ (to meet the theoretical constraints, as in the right panel of Fig. 1).

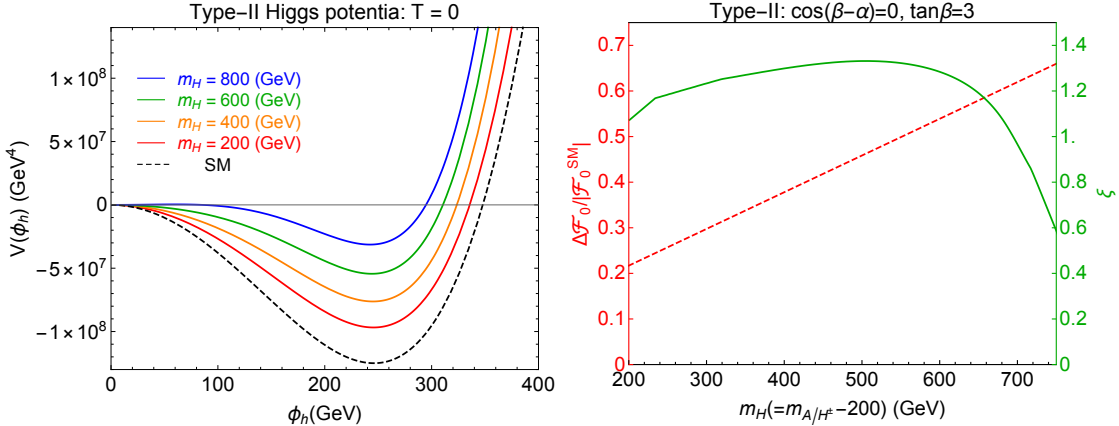


Figure 3. Zero temperature Higgs potential and its connection with the electroweak phase transition. (left): The zero temperature Higgs potential along the $\phi_h \equiv \cos\beta\phi_1 + \sin\beta\phi_2$ direction with different m_H . (right): Vacuum energy uplifting $\Delta\mathcal{F}_0/|\mathcal{F}_0^{\text{SM}}|$ and wash-out parameter ξ_c as functions of m_H .

The one-loop level Higgs vacuum uplifting in the alignment limit $\cos(\beta - \alpha) = 0$ has been given in Ref [55]:

$$\Delta\mathcal{F}_0 = \frac{1}{64\pi^2} \left[(m_h^2 - 2M^2)^2 \left(\frac{3}{2} + \frac{1}{2} \log \left[\frac{4m_A m_H m_{H^\pm}^2}{(m_h^2 - 2M^2)^2} \right] \right) \right]$$

$$+\frac{1}{2} \left(m_A^4 + m_H^4 + 2m_{H^\pm}^4 \right) + (m_h^2 - 2M^2) (m_A^2 + m_H^2 + 2m_{H^\pm}^2) \Big] \quad (4.16)$$

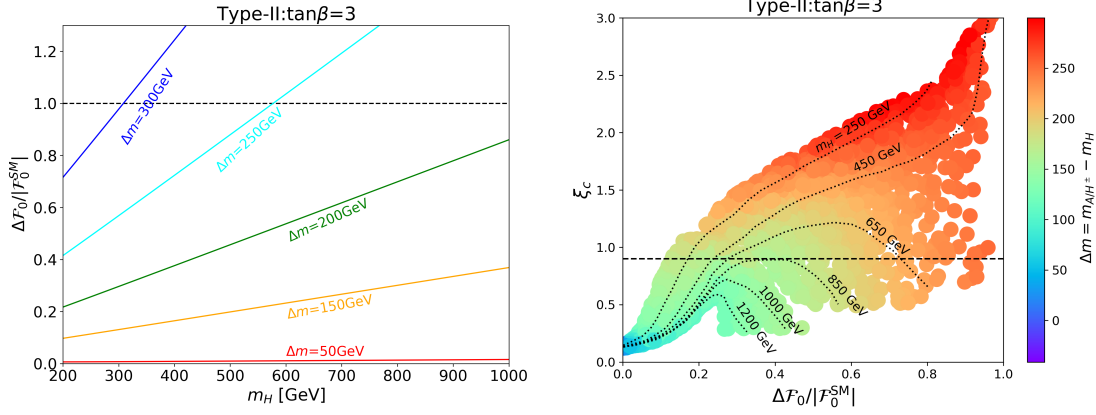


Figure 4. (left): $\Delta\mathcal{F}_0/|\mathcal{F}_0^{\text{SM}}|$ as functions of m_H , with different mass splitting. (right): Scan result projected in the $\Delta\mathcal{F}_0/|\mathcal{F}_0^{\text{SM}}| - \xi_c$ plane. Points with different mass splitting are tagged by different colors, and the dotted lines mark the CP-even Higgs mass m_H .

To illustrate the idea underlying Higgs vacuum uplifting, here we display the whole shape of the zero temperature Higgs potential. In the left panel of Fig. 3, we present the zero temperature Higgs potential along the $\phi_h \equiv \cos\beta\phi_1 + \sin\beta\phi_2$ direction, with $m_H = 200, 400, 600, 800$ GeV represented by red, orange, green and blue lines respectively. The SM Higgs potential is also shown with black dashed line for comparison. It is clear that as m_H increases, the height of the minimum point of the Higgs potential continues to rise, and the shape of the Higgs potential becomes shallower. For large m_H , $\mathcal{F}_0 > 0$, generating an unstable vacuum. Thus for a stable vacuum m_H cannot be too large.

To find the relationship between ξ_c and $\Delta\mathcal{F}_0/|\mathcal{F}_0^{\text{SM}}|$, in the right panel of Fig. 3 we present both $\Delta\mathcal{F}_0/|\mathcal{F}_0^{\text{SM}}|$ and ξ_c as functions of m_H . In the plot, the left y axis is for $\Delta\mathcal{F}_0/|\mathcal{F}_0^{\text{SM}}|$ with the red dashed line representing the relationship with m_H . While ξ_c , the right y axis, is shown by the solid green line. Here ξ_c is calculated numerically from the package BSMPT.

As the red dashed line, it is clear that there is a linear relationship between $\Delta\mathcal{F}_0/|\mathcal{F}_0^{\text{SM}}|$ and m_H , similar as the left panel. But as the green line shows, ξ_c is not monotonically dependent on m_H and gets the maximum value around $m_H = 500$ GeV. This result can be understood by our high temperature expansion analysis. Generally as m_H , equal to M^2 in our scenario to meet theoretical constraints, becomes too large, the non-SM Higgs mass is dominated by M^2 and $E_{(H/A/H^\pm)}$ get smaller as Eq.(4.13). Thus the phase transition strength becomes weaker as m_H increases from Eq.(4.7) and Eq.(4.1).

Since $\Delta\mathcal{F}_0/|\mathcal{F}_0^{\text{SM}}|$ always gets larger when m_H grows, while ξ_c gets larger at first ($m_H < 500$ GeV here), and then gets smaller, we can conclude $\Delta\mathcal{F}_0/|\mathcal{F}_0^{\text{SM}}|$ is not monotonically correlated with ξ_c . This conclusion is different to the previous study [46].

In order to get a more robust relationship between $\Delta\mathcal{F}_0/|\mathcal{F}_0^{\text{SM}}|$ and ξ_c , as well as exploring the mass splitting effects $\Delta m = m_{A/H^\pm} - m_H$, we extend the benchmark case by including different mass splittings between the non-SM Higgs bosons:

$$\begin{aligned} \tan\beta &= 3.0, \quad \cos(\beta - \alpha) = 0, \quad m_H \in (200, 1000) \text{ GeV}, \\ \sqrt{\lambda v^2} &= 0, \quad \Delta m = m_{A/H^\pm} - m_H \in (0, 300) \text{ GeV}. \end{aligned} \quad (4.17)$$

The reason for us to consider different mass splittings is that the mass splitting between different non-SM Higgs bosons is roughly proportional to the size of the couplings λ_i . Generally speaking, the greater the couplings λ_i , the easier it is for the non-SM Higgs bosons to change the shape of the Higgs thermal potential from Eq. (4.13) and Eq. (4.18). However, as can be seen from Eq. (4.16), a large mass splitting tends to be more limited by vacuum stability considerations, since too large mass splitting and vacuum uplifting $\Delta\mathcal{F}_0$ can result to $\Delta\mathcal{F}_0/|\mathcal{F}_0^{\text{SM}}| > 1$. In the left panel of Fig. 4, we present $\Delta\mathcal{F}_0/|\mathcal{F}_0^{\text{SM}}|$ as a function of m_H under different mass splittings $\Delta m = m_{A/H^\pm} - m_H = 50$ (red), 150 (orange), 200 (green), 250 (cyan), and 300 (blue) GeV. It is clear that the curves with the largest mass splittings quickly reach the unstable limit $\Delta\mathcal{F}_0 = |\mathcal{F}_0^{\text{SM}}|$ as m_H increases. In the right panel of Fig. 4, we present our scan results in the plane of $\Delta\mathcal{F}_0/|\mathcal{F}_0^{\text{SM}}| - \xi_c$. Points with different mass splittings are tagged by different colors, with m_H indicated by black dotted lines.

To understand our scan results, we need to invoke the analysis we performed in the last subsection. In our scenario, we have the following relationships between different parameters:

$$\lambda_{A/H^\pm} v^2 = (\Delta m)^2 + 2m_H \Delta m \quad (4.18)$$

with $\Delta m = m_{A/H^\pm} - m_H, m_H^2 = M^2$. Thus, following the discussion we presented in the last subsection, if the value of Δm is fixed and m_H is not too large, the phase transition strength will increase as m_H and $\Delta\mathcal{F}_0/|\mathcal{F}_0^{\text{SM}}|$ increase. But if m_H becomes too large and dominates m_{A/H^\pm} , the phase transition strength will decrease as m_H increases, until the vacuum becomes unstable, i.e. $\Delta\mathcal{F}_0 = |\mathcal{F}_0^{\text{SM}}|$. In the right panel of Fig. 4, we therefore observe that ξ_c first rises as $\Delta\mathcal{F}_0 = |\mathcal{F}_0^{\text{SM}}|$ increases (equivalent to m_H increasing), and then ξ_c decreases as $\Delta\mathcal{F}_0 = |\mathcal{F}_0^{\text{SM}}|$ (and m_H) continues to increase.

For the right panel of Fig. 4, depending on the mass splitting and the phase transition features, we can divide the parameter space into three regions:

1. The small mass splitting region, with mass splitting $\Delta m < 160\text{GeV}$. In this case, the Higgs vacuum energy cannot be uplifted too high, which means that these points are safe from vacuum stability bounds, and m_H can vary from 200GeV to 1TeV. Due to the small value of Δm , however, $\lambda_{A/H^\pm} v^2$ is too small to satisfy the requirement of a SFOEWPT.
2. The medium mass splitting region, with mass splitting $\Delta m \in [160\text{GeV}, 230\text{GeV}]$. In this case, most of the parameter space is still safe from the vacuum stability constraint.

When m_H is not too large, it helps to enhance the phase transition strength. As m_H grows to dominate the mass expression of m_{A/H^\pm} , ξ_c rapidly decreases. We also observe that ξ_c rises firstly and then falls as $\Delta\mathcal{F}_0/|\mathcal{F}_0^{\text{SM}}|$ increases. The middle region of $\Delta\mathcal{F}_0/|\mathcal{F}_0^{\text{SM}}|$ is favored by the existence of a SFOEWPT.

3. The large mass splitting region, with mass splitting $\Delta m > 230\text{GeV}$. In this region $\Delta\mathcal{F}_0/|\mathcal{F}_0^{\text{SM}}|$ starts from a value that is larger than 0.4, and quickly touches the vacuum stability bound $\Delta\mathcal{F}_0/|\mathcal{F}_0^{\text{SM}}| = 1$ as m_H increases. This means that, before m_H has increased to be able to dominate m_{A/H^\pm} , the vacuum is already unstable. We therefore observe that ξ_c increases nearly monotonically as $\Delta\mathcal{F}_0/|\mathcal{F}_0^{\text{SM}}|$ increasing.

Through the above discussion, it is clear that the upper limits on the non-SM Higgs boson masses in the 2HDM come from vacuum stability (when the mass splitting is large), or the SFOEWPT requirement (when the mass splitting is medium-large). Without the SFOEWPT requirement, the non-SM Higgs bosons can be arbitrarily heavy without violating vacuum stability, provided the mass splitting between them is small enough.

On the other hand, the black dotted lines in the right panel of Fig. 4 clearly show the relationship between ξ_c and m_H . We found that ξ_c is a monotonically increasing function of $\Delta\mathcal{F}_0/|\mathcal{F}_0^{\text{SM}}|$ when $m_H < 500\text{ GeV}$, such as $m_H = 250, 450\text{ GeV}$ in the right panel of Fig. 4. But with larger mass, the phase transition strength ξ_c gets smaller, and when $m_H > 850\text{ GeV}$, ξ_c can no longer reach 0.9. To avoid the unstable vacuum, larger m_H needs smaller Δm as in Fig. 3. Therefore, a too large m_H will result in a too small $\lambda_{A/H^\pm}v^2$, which could not generate a SFOEWPT. In Table 1 we present the range of Δm and $\Delta\mathcal{F}_0/|\mathcal{F}_0^{\text{SM}}|$ for different values of m_H . This clearly shows that the SFOEWPT-satisfied region keeps shrinking as m_H gets larger and larger.

$m_H(\text{ GeV})$	250	450	650	700	850
$\Delta m(\text{ GeV})$	(170, 280)	(160, 280)	(150, 230)	(155, 210)	(160, 165)
$\Delta\mathcal{F}_0/ \mathcal{F}_0^{\text{SM}} $	(0.18, 0.83)	(0.25, 0.95)	(0.28, 0.73)	(0.3, 0.7)	(0.38, 0.42)

Table 1. The parameter space for which a SFOEWPT is obtained, with $\tan\beta = 3$, $\Delta m = m_{A/H^\pm} - m_H$ in the Type-II 2HDM, similar to Fig. 4.

4.2 Case1: alignment limit with fixed mass splitting

Following the previous approximate analysis of the electroweak phase transition, we now investigate a series of benchmark cases, starting with,

$$\begin{aligned} \tan\beta &\in (0.2, 50), \quad m_H \in (200, 1000)\text{ GeV}, \\ \cos(\beta - \alpha) &= 0, \quad \sqrt{\lambda}v^2 = 0, \quad \Delta m = m_{A/H^\pm} - m_H = 200\text{ GeV}. \end{aligned} \quad (4.19)$$

Here we take $\sqrt{\lambda}v^2 = 0$ to allow for the largest range of $\tan\beta$ as shown in the second and third panel of Fig. 1. To explore the dependence on m_H , we fix the mass splitting $\Delta m = 200\text{ GeV}$,

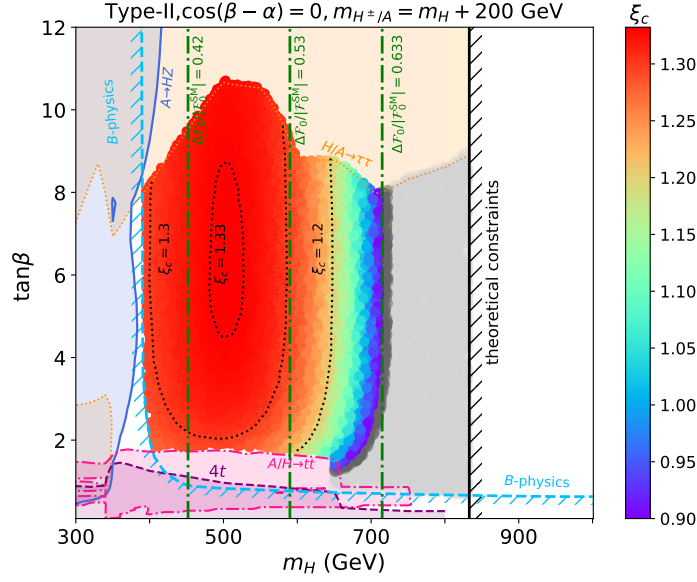


Figure 5. Electroweak phase transition and other constraints analyzed in the plane of $m_H - \tan \beta$ for the Type-II 2HDD. Here we fix $\Delta m = m_{A/H^\pm} - m_H = 200$ GeV and assume the tree-level alignment limit $\cos(\beta - \alpha) = 0$, which is same as the right panel of Fig. 2. The central colored region is allowed after all constraints. The null results of $H/A \rightarrow \tau\tau$ searches (orange region with dotted line boundary) provide an upper bound on $\tan \beta$ for a given m_H , the $A \rightarrow HZ$ results (blue region) constrain the small mass region, and the $A/H \rightarrow tt$ (red region with dash-dotted line boundary) and $4t$ (purple region with dashed line boundary) channels constrain the small $\tan \beta$ region. The hatched cyan dashed line show the constraints from B physics observables, and the hatched black line indicates the theoretical constraints. The gradient-filled regions show the parameter space that can generate a SFOEWPT, with the black dashed lines indicating the phase transition strength ξ_c . The black region means there is an electroweak phase transition with $\xi_c < 0.9$. The grey regions are allowed by various constraints, but there is no first order phase transition. We also show $\Delta\mathcal{F}_0/|\mathcal{F}_0^{\text{SM}}|$ by green dash-dotted lines.

and assume the tree-level alignment limit $\cos(\beta - \alpha) = 0$. The parameter space is the same as the right panel of Fig. 2, where there are important constraints from direct non-SM Higgs boson searches at LHC Run-II including $H/A \rightarrow \tau\tau$ (orange region with dotted line boundary, providing an upper bound), $A \rightarrow HZ$ (blue region, constraining the small mass region), and $A/H \rightarrow tt$ (red region with dash-dotted line boundary) and $4t$ (purple region with dashed line boundary), which constrain the small $\tan \beta$ region. For the Type-II 2HDM, there are important constraints on the mass of the charged Higgs boson from B physics, which are represented by the hatched cyan dashed line. B physics observables also give effective constraints at small $\tan \beta$. The hatched black line indicates the theoretical constraints, as discussed in Fig. 1, requiring $m_H < 835$ GeV for $\cos(\beta - \alpha) = 0$.

After these theoretical and experimental constraints, the allowed parameter region is approximately located around $m_H \in (380, 830)$ GeV, and $\tan \beta \in (1, 10)$. The colored region $m_H \in (380, 700)$ GeV shows the parameter space which can generate a SFOEWPT, with

dashed lines indicating the phase transition strength ξ_c . We can see that, generally, the strength ξ_c gets its maximal value around $m_H = 500$ GeV, which is discussed in the right panel of Fig. 3. The green dash-dotted lines show $\Delta\mathcal{F}_0/|\mathcal{F}_0^{\text{SM}}| = 0.42, 0.53, 0.63$, which grows with larger m_H and is independent of $\tan\beta$. We can therefore again conclude that the SFOEWPT strength is not monotonically dependent on m_H or $\Delta\mathcal{F}_0/|\mathcal{F}_0^{\text{SM}}|$.

Finally there is a black band region round $m_H = 700$ GeV, which means that the phase transition strength $\xi_c < 0.9$. Beside the black band region, there is a grey region which is allowed by various constraints, but ξ_c in this region has no value. This is because the phase transition in this region is not first order, and thus we can not find the critical temperature and calculate ξ_c . We have also checked that Higgs and Z-pole precision measurements give no constraints in this case since $\cos(\beta - \alpha) = 0$ and $\Delta m = 200$ GeV.

4.3 Case2: alignment limit with $m_A = m_{H^\pm}$

Based on the results in Fig. 4, here we show our second benchmark case, the alignment limit with fixed $\tan\beta$,

$$\begin{aligned} m_{A/H^\pm} &\in (500, 1200) \text{ GeV}, \quad m_H \in (200, 1000) \text{ GeV}, \\ \cos(\beta - \alpha) &= 0, \quad \sqrt{\lambda v^2} = 0, \quad \tan\beta = 3. \end{aligned} \quad (4.20)$$

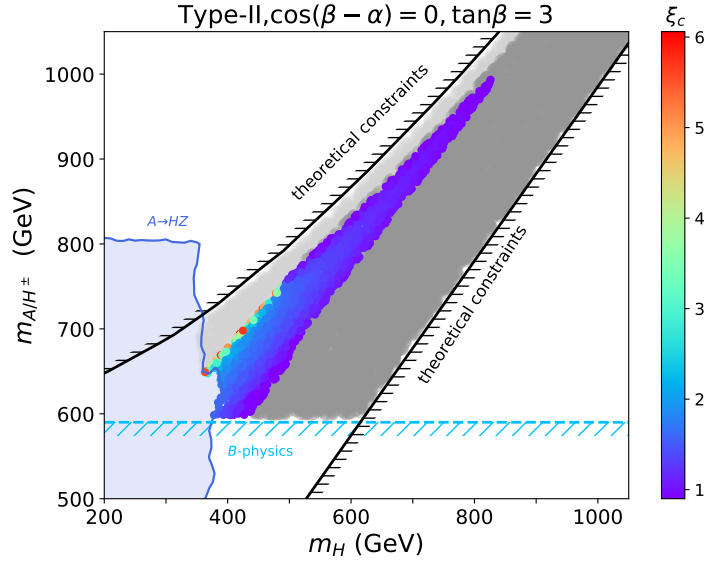


Figure 6. Electroweak phase transition and other constraints analyzed in the plane of $m_H - m_{A/H^\pm}$, with $\cos(\beta - \alpha) = 0$ and $\tan\beta = 3$, for the Type-II 2HDM. Of the various heavy Higgs search channels, only $A \rightarrow HZ$ gives visible constraints, shown by the blue region. Again the hatched cyan dashed line shows the B -physics constraints, and the hatched black lines are for theoretical constraints. The allowed regions are divided into three parts, the colorful region with $\xi_c > 0.9$, the light grey region (mostly above the colorful region) with $\xi_c < 0.9$, and the dark grey region in which a SFOEWPT cannot occur.

Again here $\sqrt{\lambda v^2} = 0$ is set to avoid the constraints on the parameter $\tan \beta$. In Eq. (4.2), we show the constraints arising from the requirement of a SFOEWPT and other observables in the $m_H - m_{A/H^\pm}$ plane of the Type-II 2HDM. For the various heavy Higgs search channels, only $A \rightarrow HZ$ gives a visible constraint (shown by the blue region), which can exclude the region with $m_H < 350$ GeV, $m_{A/H^\pm} < 800$ GeV. B -physics constraints, shown by the hatched cyan dashed line, exclude $m_{H^\pm} < 580$ GeV. Since here we have $m_A = m_{H^\pm}$ and $\cos(\beta - \alpha) = 0$, the Higgs and Z-pole precision constraints are satisfied automatically. On the other hand, the theoretical constraints, indicated by hatched black lines, give a strong limit on the mass splitting range, roughly $\Delta m = m_{A/H^\pm} - m_H \in (-50, 200)$ GeV.

The allowed regions are divided into three parts, the colorful region with $\xi_c > 0.9$, the light grey region which is mostly above the colorful region with $\Delta m = m_{A/H^\pm} - m_H \approx 200$ GeV.) with $\xi_c < 0.9$, and the dark grey region in which a phase transition cannot occur. From the colored region, we find that, both a too large or too small Δm will not allow for a SFOEWPT. As discussed in Fig. 4, for a too small Δm , the Higgs vacuum energy cannot be uplifted high enough to generate a phase transition, while too large a value of Δm will result in an unstable potential $\mathcal{F}_0 = |\mathcal{F}_0^{\text{SM}}|$, where the potential at second EW minimal is higher than the it at the origin. This is also responsible for the upper limit on m_H , as the analysis around Eq. (4.18) shows, since too small a value of $m_H \Delta m$ cannot generate a proper barrier for a SFOEWPT.

4.4 Case3: alignment limit with $m_H=700$ GeV

In our previous case studies, we always had the simple assumption of $m_A = m_{H^\pm}$ to satisfy the oblique constraints from Z-pole measurements, and also to simplify the parameter space. Here to study the general mass splitting region, we take another benchmark case,

$$m_A \in (500, 1200) \text{ GeV}, \quad m_{H^\pm} \in (500, 1200) \text{ GeV}, \\ m_H = 700 \text{ GeV}, \quad \cos(\beta - \alpha) = 0, \quad \sqrt{\lambda v^2} = 0, \quad \tan \beta = 3.$$

$\sqrt{\lambda v^2} = 0$ is once more set to avoid the constraints on the parameter $\tan \beta$, and we take $m_H = 700$ GeV as an example. In Eq. (4.3), we show the electroweak phase transition and other constraints in the plane of $m_A - m_{H^\pm}$ in the Type-II 2HDM. The theoretical constraints are now particularly important, as the region with hatched black lines acts as a boundary on the allowed parameter space. The lower limits on both m_A and m_{H^\pm} are approximately 670 GeV, while the upper limits are 970 and 930 GeV respectively. This is because, once there is a large mass splitting, λ_{1-5} will be enlarged [178]. For the various new physics search channels, only the oblique constraints make an effect here. As the hatched blue dashed lines show, the allowed regions are around either $m_A = m_{H^\pm}$ or $m_{H^\pm} = m_H = 700$ GeV.

The allowed regions are divided into three parts, the colorful region with $\xi_c > 0.9$ allowing a SFOEWPT, the light grey region (mostly above the colorful region) with $\xi_c < 0.9$, and the dark grey region without a first order phase transition. To understand the features here, we also have green dash-dotted lines for $\Delta \mathcal{F}_0 / |\mathcal{F}_0^{\text{SM}}|$, which gets large when m_A, m_{H^\pm} increases.

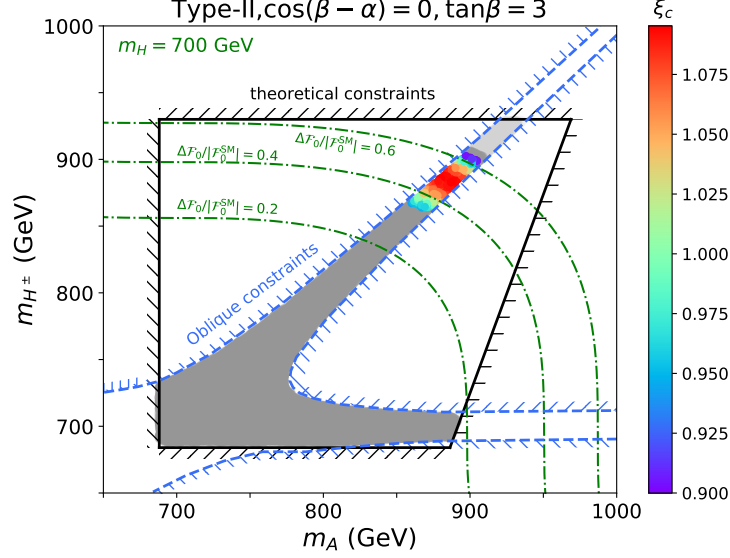


Figure 7. Electroweak phase transition and other constraints analyzed in the plane of $m_A - m_{H^\pm}$, with $\cos(\beta - \alpha) = 0$ and $\tan \beta = 3$, in the Type-II 2HDM. For the various new physics search channels, only the oblique constraints make an important contribution, represented by the hatched blue dashed lines. Theoretical constraints are shown by the hatched black lines. The allowed regions are divided into three parts, the colorful region with $\xi_c > 0.9$, the light grey region (mostly above the colorful region) with $\xi_c < 0.9$, and the dark grey region where a first order phase transition does not occur. We also show green dash-dotted lines for $\Delta \mathcal{F}_0 / |\mathcal{F}_0^{\text{SM}}|$.

We also note that, to get a proper vacuum energy uplifting, at least one of m_A or m_{H^\pm} should be large. For instance, $\mathcal{F}_0 / |\mathcal{F}_0^{\text{SM}}| = 0.4$ requires $m_{H^\pm} = 900$ GeV when $m_A = m_H$, or $m_A = 950$ GeV when $m_A = m_{H^\pm}$, or $m_A \approx m_{H^\pm} \approx 870$ GeV. The region with $\xi_c > 0.9$ is located at $\mathcal{F}_0 / |\mathcal{F}_0^{\text{SM}}| \in (0.37, 0.63)$. The large mass limit comes from $\mathcal{F}_0 / |\mathcal{F}_0^{\text{SM}}| \rightarrow 1$, where the vacuum is not stable, while the small mass limit comes from Eq. (4.18), where there is only limited vacuum uplifting and a barrier to generating a SFOEWPT.

4.5 General results

During the last section, we presented three benchmark cases to discuss the effects of the heavy Higgs masses on the existence of a SFOEWPT in the alignment limit, as well as the influence of a variety of theoretical and current experimental constraints up to the one-loop level.

In this section, we present a more general study of Type-I and Type-II 2HDMs. At the same time, we will explore the impact of future results from Higgs factories, presented in Section 3.3, taking the CEPC precision measurements as an example.

Our parameter scan regions for both Type-I and Type-II are :

$$|\alpha| < \frac{\pi}{2}, \tan \beta \in (0.2, 50), m_A \in (10, 1500) \text{ GeV}, m_{H^\pm} \in (10, 1500) \text{ GeV}, \\ m_{12}^2 \in (0, 1500^2) \text{ GeV}^2, m_h = 125.1 \text{ GeV}, m_H \in (130, 1500) \text{ GeV}. \quad (4.21)$$

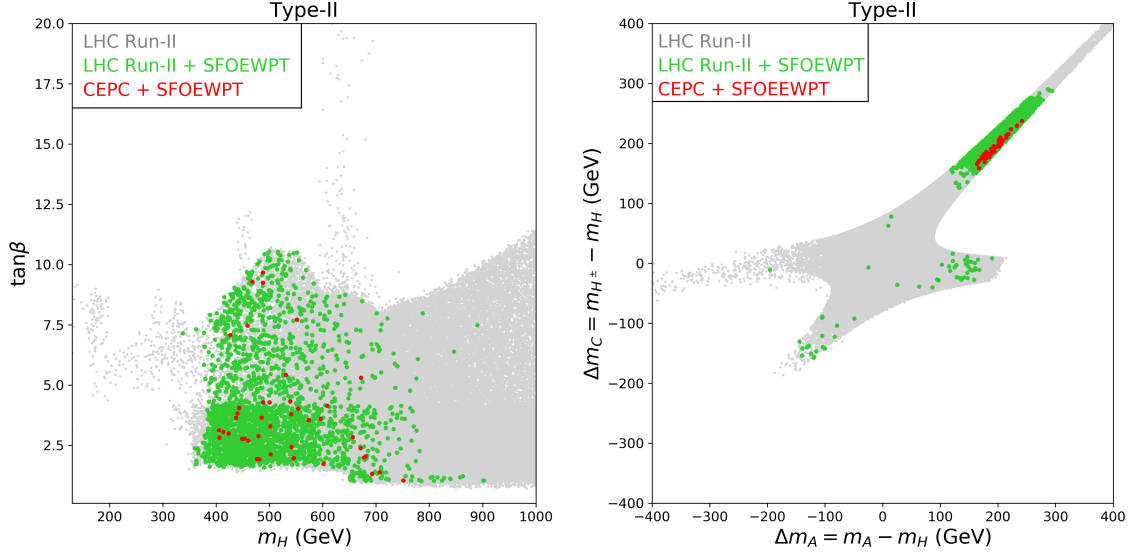


Figure 8. The allowed parameter space in the plane of $m_H - \tan \beta$ (left), $\Delta m_A - \Delta m_C$ (right). The grey points survive all theoretical and current experimental constraints. The green ones are able to provide a SFOEWPT, while the red ones are allowed by future precision measurements from CEPC.

We perform a random parameter scan in the above parameter region, with the total number of samples exceeding 1 billion, for both Type-I and Type-II models.

In Fig. 8 we show the scan results for the Type-II 2HDM. The grey scatter points are the regions allowed by B physics, theoretical constraints, heavy Higgs direct searches and SM Higgs precision measurements at the current LHC Run-II, and constraints from EW oblique operators. The green points are a subset of the grey ones, which can generate a SFOEWPT, and the red points are further required to meet the constraints from future Higgs precision measurements at CEPC. Compared to **Case 1** (Section 4.2), which assumed the alignment limit and set $m_{H^\pm} = m_A$, here we could divide the whole allowed region into 4 classes,

- **Class A:** Regions with $m_H < 350$ GeV. Here the region has $m_{H^\pm} \approx m_A > m_H$, and the mass splitting is about (300,500) GeV to meet the constraint $m_{H^\pm} > 580$ GeV. Generally $\sqrt{\lambda v^2} \approx 0$ to allow for such a large mass splitting and $\tan \beta$ is within the region selected by the theoretical constraints shown in Fig. 1. This region can also be divided into two subgroups based on $\text{sign}(\kappa_b)$. When $\text{sign}(\kappa_b) = +$, $m_H < 200$ GeV, $\tan \beta \in (5, 10)$ can escape the constraints from the $H \rightarrow \tau\tau$ channel as in the right panel of Fig. 2. At the same time, the large mass splitting $m_A - m_H > 450$ GeV weakens the constraint from the $A \rightarrow HZ$ channel [132]. Another subgroup is $\text{sign}(\kappa_b) = -$, the so-called wrong-sign Yukawa coupling region with $\cos(\beta - \alpha) \approx 2/\tan \beta$. Here m_H can reach 350 GeV, $\cos(\beta - \alpha) \in (0.2, 0.4)$, and LHC direct searches require $\tan \beta < 10$ [142]. Because of the large mass splitting in this region, $\Delta \mathcal{F}_0/|\mathcal{F}_0^{\text{SM}}|$ is too large to produce a stable vacuum.

- **Class B:** Regions with $5 < \tan \beta < 12$ for $m_H \approx 450$ GeV. This region is also a wrong-sign Yukawa coupling region with $\text{sign}(\kappa_b) = -$. Generally $\sqrt{\lambda v^2} \approx 0$ to meet theoretical constraints, and $m_{H^\pm} \approx m_A = m_H + 140$ GeV with $\tan \beta < 12$ to meet constraints from the $A \rightarrow HZ$ and $A/H \rightarrow \tau\tau$ channels (see Fig. 2). $m_{A/H^\pm} - m_H > 140$ GeV to meet B physics constraints, while a larger mass splitting is not allowed by theoretical constraints even though $\sqrt{\lambda v^2} \approx 0$. As the right panel of Fig. 4 shows, because $m_H = 450$ GeV and $\Delta m = 140$ GeV, $|\Delta\mathcal{F}_0/\mathcal{F}_0^{\text{SM}}| < 0.2$ is too small, thus the vacuum uplifting is too small, and there is no SFOEWPT here.
- **Class C:** Regions with $5 < \tan \beta < 45$ for $600 < m_H < 700$ GeV. Here $m_{H^\pm} = m_H$ with $m_A < m_h = 125$ GeV. Again it is a wrong-sign Yukawa coupling region with $\sqrt{\lambda v^2} \approx 0$. The lower limit of m_H comes from B physics and EW oblique constraints, and the upper limit comes from theoretical constraints $m_H - m_A < 650$ GeV. In the region, $|\Delta\mathcal{F}_0/\mathcal{F}_0^{\text{SM}}| < 0$, thus there is no chance to generate a SFOEWPT.
- **Class D:** The main allowed region with $m_H > 350$ GeV. The region is similar to the white allowed region in the right panel of Fig. 2. Compared to **Case 1** with $m_{H^\pm} = m_A = m_H = 200$ GeV in the alignment limit, here the allowed grey region by current LHC Run-II has no upper limit on m_H anymore from theoretical constraints when all parameters are free. When $m_H < 900$ GeV, $1 < \tan \beta < 10$ is required to satisfy the constraints from $H/A \rightarrow \tau\tau$, top searches and B physics. When $m_H > 900$ GeV, $\tan \beta$ can take a larger value as the constraining power of the $H/A \rightarrow \tau\tau$ channel gets weaker. In this region, there are a number of points with $\xi_c > 0.9$, as shown by green points. We can see the green parameter space has an upper limit of about 900 GeV. For points that also satisfy CEPC constraints as the red points, the parameter space has an upper limit of about 800 GeV.

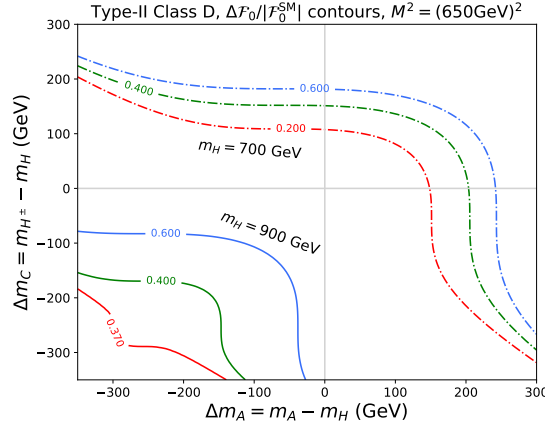


Figure 9. $|\Delta\mathcal{F}_0/\mathcal{F}_0^{\text{SM}}|$ contours in the plane of $\Delta m_A - m_C$ to explore **Class D**. Here $M^2 = \frac{m_{12}^2}{\sin \beta \cos \beta} = (650 \text{ GeV})^2$, $m_H = 900$ GeV (solid lines), 700 GeV (dashed lines).

The right panel of Fig. 8 shows the scan results in the plane of $\Delta m_A = m_A - m_H$ and $\Delta m_C = m_A - m_{H^\pm}$, allowing us to analyze the **Class D** parameter space. Here the general structure is $\Delta m_C \approx \Delta m_A$ or $\Delta m_C = 0$ because of Z-pole oblique constraints.

For the green points from **Class D** that satisfy LHC Run-II constraints whilst producing a SFOEWPT, there are mainly three regions. For **Class D1**, $\Delta m_C \approx \Delta m_A \in (100, 350)$ GeV. The region has $m_H \in (350, 600)$ GeV, $\sqrt{\lambda v^2} \approx 0$, $\tan \beta \in (1, 5)$, and the features are similar to **Case 3** results in Section 4.4. For **Class D2**, $\Delta m_C \approx \Delta m_A \in (-200, -50)$ GeV. The region has $m_H \in (750, 900)$ GeV, $M^2 = \frac{m_{12}^2}{\sin \beta \cos \beta} \approx (650 \text{ GeV})^2$, $\tan \beta \approx 1$. In the left panel of Fig. 9, we show the $\Delta \mathcal{F}_0 / |\mathcal{F}_0^{\text{SM}}|$ contours in the plane of $\Delta m_A - m_C$. We can see that when $m_H = 900$ GeV and $M = 650$ GeV, $\Delta m_C \approx \Delta m_A \in (-200, -50)$ GeV, which results in $\Delta \mathcal{F}_0 / |\mathcal{F}_0^{\text{SM}}| \in (0.37, 0.6)$. This is one of the essential conditions for a SFOEWPT. In this region, $\sqrt{\lambda v^2} \in (500, 600)$ GeV, thus theoretical constraints impose $\tan \beta \approx 1$ as shown in Fig. 1. For **Class D3**, $\Delta m_C \approx 0$, $\Delta m_A \in (50, 200)$ GeV. The region has $m_H \in (650, 750)$ GeV, $M^2 = \frac{m_{12}^2}{\sin \beta \cos \beta} \approx (650 \text{ GeV})^2$, $\tan \beta \approx 1$, $\sqrt{\lambda v^2} \in (450, 550)$ GeV. Similarly in the left panel of Fig. 9, we show the $\Delta \mathcal{F}_0 / |\mathcal{F}_0^{\text{SM}}|$ contours for $m_H = 700$ GeV with dash-dotted lines. **Class D2** and **Class D3**, which are allowed by current LHC indirect Higgs precision measurements and direct heavy Higgs searches, will be excluded by Higgs precision observables at the CEPC. This is because the large $\sqrt{\lambda v^2}$ in the two regions will lead to large one-loop level corrections to the SM-like Higgs couplings [118, 177, 178], and large mass splittings around $\tan \beta = 1$ are not allowed by precise measurements of the Higgs couplings.

We show our general scan results for the Type-I 2HDM in Fig. 10. The allowed grey, green and red points here cover a larger area than for the Type-II model, which mainly comes from heavy Higgs direct search constraints on the large $\tan \beta$ region. As the benchmark case shown in Fig. 2 shows, there is no constraint on $\tan \beta > 2$ when $m_H > 2m_t$ in the Type-I 2HDM because all $Hf\bar{f}$ couplings are reduced as $\tan \beta$ increases.

At the same time, there is also a larger range for $\cos(\beta - \alpha)$ at $\tan \beta > 2$ compared to the Type-II 2HDM [142]. Thus terms involving $\cos(\beta - \alpha)$ will also become important, and from Ref. [55] we can get,

$$\Delta \mathcal{F}_0|_{\text{general}} = \Delta \mathcal{F}_0|_{\cos(\beta-\alpha)=0} + \frac{1}{128\pi^2} \cos(\beta - \alpha) \sin(\beta - \alpha) \left(\tan \beta - \frac{1}{\tan \beta} \right) (m_H^2 - m_h^2)(2m_{H^\pm}^2 + 2m_A^2 + 5m_H^2 - 6M^2) + \mathcal{O}(\cos^2(\beta - \alpha)), \quad (4.22)$$

here $M^2 = \frac{m_{12}^2}{\sin \beta \cos \beta}$. Because of this additional term, once there is sizable $\tan \beta, \cos(\beta - \alpha)$, the allowed $\Delta m_A, \Delta m_C$ to generate the proper $\Delta \mathcal{F}_0 / |\mathcal{F}_0^{\text{SM}}|$ range will be a little different to that in the Type-II case. In other words, the allowed parameter space in the Type-I model is larger than that in the Type-II model.

Generally speaking, compared to the Type-II 2HDM, the upper limit of m_H allowed by a SFOEWPT in the Type-I model can still reach to 900 GeV. In the Type-II model, such points have $\Delta m_{A,C} < 0$, and are excluded by Higgs and Z-pole precision measurements. But larger $\tan \beta$ values allow larger mass splittings between the heavy Higgs bosons [177, 178], and thus

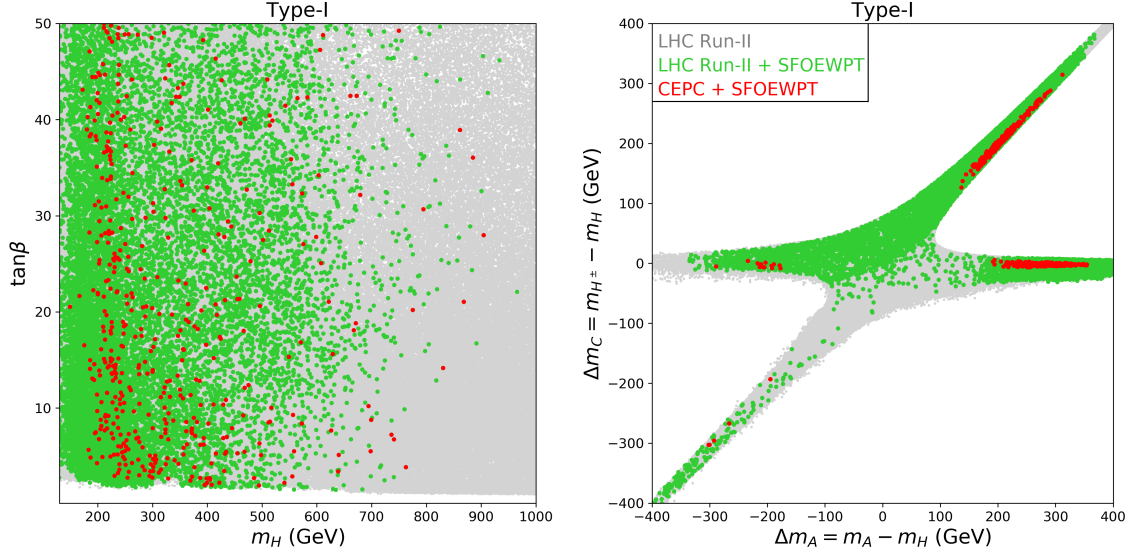


Figure 10. Allowed parameter space in the plane of $m_H - \tan \beta$ (left), $\Delta m_A - \Delta m_C$ (right). Same as Fig. 8, but for the Type-I model.

in the Type-I model $m_H \rightarrow 900$ GeV still satisfy these precision measurements. Similarly the regions with $\Delta m_C \approx 0, \Delta m_A < 0$ or $\Delta m_C \approx 0, \Delta m_A > 0$ which are not allowed in the Type-II model can still generate a SFOEWPT in the Type-I model.

5 Conclusion

In this work, we have revisited the existence of a strong first order electroweak phase transition (SFOEWPT) in the Type-I and Type-II 2HDMs. Using both numerical and analytical analysis methods, we pointed out that $\Delta \mathcal{F}_0 / |\mathcal{F}_0^{\text{SM}}|$ is not monotonically related to ξ_c as shown in Fig. 3 and Fig. 4. This conclusion is different to that of a previous study [46].

We also found, SFOEWPT suggests the non-SM Higgs bosons, $H/A/H^\pm$, have upper limits on their mass as our benchmark **Case 1** Section 4.2 and general scan results Fig. 8 and Fig. 10. This limits comes from the combined requirements of vacuum stability at zero temperature and $\lambda_{H/A/H^\pm} v^2$ corrections term at high temperature.

By combining current bounds from LHC direct and indirect Higgs searches, current electroweak precision measurements, flavour physics, and anticipated precision measurements at the future CEPC Z and Higgs factory, we have shown that the requirement of a SFOEWPT puts strong constraints on the mass spectrum of $H/A/H^\pm$:

$$\text{For the type-I 2HDM:} \quad (5.1)$$

$$200 \text{ GeV} \lesssim m_H, m_A, m_{H^\pm} \lesssim 1 \text{ TeV}, |m_A - m_H| \in (150 \text{ GeV}, 350 \text{ GeV}) \\ |m_{H^\pm} - m_H| \in (150 \text{ GeV}, 350 \text{ GeV})$$

$$\text{For the type-II 2HDM:} \quad (5.2)$$

$$400 \text{ GeV} \lesssim m_H, m_A, m_{H^\pm} \lesssim 1 \text{ TeV}, m_A - m_H \in (150\text{GeV}, 250\text{GeV})$$

$$m_{H^\pm} - m_H \in (150\text{GeV}, 250\text{GeV})$$

In Type-II 2HDM, parameter space **Class D2** ($m_A = m_{H^\pm} < m_H$) and **D3** ($m_A < m_{H^\pm} = m_H$) are allowed by SM Higgs precision measurements and heavy Higgs searches at LHC Run-II, but can be excluded by Higgs precision observables at the CEPC because of the one-loop level corrections to the SM-like Higgs couplings. The allowed region has $m_A = m_{H^\pm} > m_H$ and small $\lambda v^2 = m_H^2 - \frac{m_{12}^2}{\sin\beta \cos\beta}$. In Type-I 2HDM, because of allowed large $\tan\beta$ region from Higgs precision measurements, **Class D2** and **D3** are still allowed.

Both Type-I and Type-II requires a sizable mass splitting between different heavy non-SM Higgs. And the suggested upper limits of $m_{A/H/H^\pm}$ is 900 GeV at current stage, and 800 GeV after including Higgs and Z-pole precisions at CEPC. Such a constrained spectrum points out a clear direction for direct searches at the LHC and future colliders.

Acknowledgments

We thank Martin White for useful discussion and a careful reading of the manuscript. WS and AGW are supported by the Australian Research Council (ARC) Centre of Excellence for Dark Matter Particle Physics (CE200100008). M.Z. is supported by the National Natural Science Foundation of China (Grant No. 11947118).

References

- [1] **ATLAS** Collaboration, G. Aad et al., “Observation of a new particle in the search for the Standard Model Higgs boson with the ATLAS detector at the LHC,” [*Phys. Lett. B* **716** \(2012\) 1–29](#), [arXiv:1207.7214 \[hep-ex\]](#).
- [2] **CMS** Collaboration, S. Chatrchyan et al., “Observation of a new boson at a mass of 125 GeV with the CMS experiment at the LHC,” [*Phys. Lett. B* **716** \(2012\) 30–61](#), [arXiv:1207.7235 \[hep-ex\]](#).
- [3] A. Sakharov, “Violation of CP Invariance, C asymmetry, and baryon asymmetry of the universe,” [*Sov. Phys. Usp.* **34** \(1991\) no. 5, 392–393](#).
- [4] V. Kuzmin, V. Rubakov, and M. Shaposhnikov, “On the Anomalous Electroweak Baryon Number Nonconservation in the Early Universe,” [*Phys. Lett. B* **155** \(1985\) 36](#).
- [5] M. Shaposhnikov, “Possible Appearance of the Baryon Asymmetry of the Universe in an Electroweak Theory,” [*JETP Lett.* **44** \(1986\) 465–468](#).
- [6] M. Shaposhnikov, “Baryon Asymmetry of the Universe in Standard Electroweak Theory,” [*Nucl. Phys. B* **287** \(1987\) 757–775](#).
- [7] N. Manton, “Topology in the Weinberg-Salam Theory,” [*Phys. Rev. D* **28** \(1983\) 2019](#).
- [8] F. R. Klinkhamer and N. Manton, “A Saddle Point Solution in the Weinberg-Salam Theory,” [*Phys. Rev. D* **30** \(1984\) 2212](#).
- [9] P. Huet and E. Sather, “Electroweak baryogenesis and standard model CP violation,” [*Phys. Rev. D* **51** \(1995\) 379–394](#), [arXiv:hep-ph/9404302](#).
- [10] K. Kajantie, M. Laine, K. Rummukainen, and M. E. Shaposhnikov, “Is there a hot electroweak phase transition at $m(H)$ larger or equal to $m(W)$?,” [*Phys. Rev. Lett.* **77** \(1996\) 2887–2890](#), [arXiv:hep-ph/9605288](#).
- [11] F. Csikor, Z. Fodor, and J. Heitger, “Endpoint of the hot electroweak phase transition,” [*Phys. Rev. Lett.* **82** \(1999\) 21–24](#), [arXiv:hep-ph/9809291](#).
- [12] M. Trodden, “Electroweak baryogenesis,” [*Rev. Mod. Phys.* **71** \(1999\) 1463–1500](#), [arXiv:hep-ph/9803479](#).
- [13] T. Konstandin, “Quantum Transport and Electroweak Baryogenesis,” [*Phys. Usp.* **56** \(2013\) 747–771](#), [arXiv:1302.6713 \[hep-ph\]](#).
- [14] M. Carena, Z. Liu, and M. Riembau, “Probing the electroweak phase transition via enhanced di-Higgs boson production,” [*Phys. Rev. D* **97** \(2018\) no. 9, 095032](#), [arXiv:1801.00794 \[hep-ph\]](#).
- [15] J. M. Cline and K. Kainulainen, “Electroweak baryogenesis and dark matter from a singlet Higgs,” [*JCAP* **01** \(2013\) 012](#), [arXiv:1210.4196 \[hep-ph\]](#).
- [16] J. M. Cline, K. Kainulainen, and D. Tucker-Smith, “Electroweak baryogenesis from a dark sector,” [*Phys. Rev. D* **95** \(2017\) no. 11, 115006](#), [arXiv:1702.08909 \[hep-ph\]](#).
- [17] M. Carena, M. Quirós, and Y. Zhang, “Electroweak Baryogenesis from Dark-Sector CP Violation,” [*Phys. Rev. Lett.* **122** \(2019\) no. 20, 201802](#), [arXiv:1811.09719 \[hep-ph\]](#).

- [18] J. M. Cline, G. Laporte, H. Yamashita, and S. Kraml, “Electroweak Phase Transition and LHC Signatures in the Singlet Majoron Model,” [*JHEP* **07** \(2009\) 040](#), [arXiv:0905.2559 \[hep-ph\]](#).
- [19] S. Profumo, M. J. Ramsey-Musolf, C. L. Wainwright, and P. Winslow, “Singlet-catalyzed electroweak phase transitions and precision Higgs boson studies,” [*Phys. Rev. D* **91** \(2015\) no. 3, 035018](#), [arXiv:1407.5342 \[hep-ph\]](#).
- [20] D. Curtin, P. Meade, and C.-T. Yu, “Testing Electroweak Baryogenesis with Future Colliders,” [*JHEP* **11** \(2014\) 127](#), [arXiv:1409.0005 \[hep-ph\]](#).
- [21] F. P. Huang and C. S. Li, “Electroweak baryogenesis in the framework of the effective field theory,” [*Phys. Rev. D* **92** \(2015\) no. 7, 075014](#), [arXiv:1507.08168 \[hep-ph\]](#).
- [22] A. V. Kotwal, M. J. Ramsey-Musolf, J. M. No, and P. Winslow, “Singlet-catalyzed electroweak phase transitions in the 100 TeV frontier,” [*Phys. Rev. D* **94** \(2016\) no. 3, 035022](#), [arXiv:1605.06123 \[hep-ph\]](#).
- [23] V. Vaskonen, “Electroweak baryogenesis and gravitational waves from a real scalar singlet,” [*Phys. Rev. D* **95** \(2017\) no. 12, 123515](#), [arXiv:1611.02073 \[hep-ph\]](#).
- [24] A. Beniwal, M. Lewicki, J. D. Wells, M. White, and A. G. Williams, “Gravitational wave, collider and dark matter signals from a scalar singlet electroweak baryogenesis,” [*JHEP* **08** \(2017\) 108](#), [arXiv:1702.06124 \[hep-ph\]](#).
- [25] G. Kurup and M. Perelstein, “Dynamics of Electroweak Phase Transition In Singlet-Scalar Extension of the Standard Model,” [*Phys. Rev. D* **96** \(2017\) no. 1, 015036](#), [arXiv:1704.03381 \[hep-ph\]](#).
- [26] C.-W. Chiang, M. J. Ramsey-Musolf, and E. Senaha, “Standard Model with a Complex Scalar Singlet: Cosmological Implications and Theoretical Considerations,” [*Phys. Rev. D* **97** \(2018\) no. 1, 015005](#), [arXiv:1707.09960 \[hep-ph\]](#).
- [27] A. Alves, T. Ghosh, H.-K. Guo, K. Sinha, and D. Vagie, “Collider and Gravitational Wave Complementarity in Exploring the Singlet Extension of the Standard Model,” [*JHEP* **04** \(2019\) 052](#), [arXiv:1812.09333 \[hep-ph\]](#).
- [28] H.-L. Li, M. Ramsey-Musolf, and S. Willocq, “Probing a scalar singlet-catalyzed electroweak phase transition with resonant di-Higgs boson production in the $4b$ channel,” [*Phys. Rev. D* **100** \(2019\) no. 7, 075035](#), [arXiv:1906.05289 \[hep-ph\]](#).
- [29] N. F. Bell, M. J. Dolan, L. S. Friedrich, M. J. Ramsey-Musolf, and R. R. Volkas, “Electroweak Baryogenesis with Vector-like Leptons and Scalar Singlets,” [*JHEP* **19** \(2020\) 012](#), [arXiv:1903.11255 \[hep-ph\]](#).
- [30] B. Grzadkowski and D. Huang, “Spontaneous CP -Violating Electroweak Baryogenesis and Dark Matter from a Complex Singlet Scalar,” [*JHEP* **08** \(2018\) 135](#), [arXiv:1807.06987 \[hep-ph\]](#).
- [31] F. P. Huang, Z. Qian, and M. Zhang, “Exploring dynamical CP violation induced baryogenesis by gravitational waves and colliders,” [*Phys. Rev. D* **98** \(2018\) no. 1, 015014](#), [arXiv:1804.06813 \[hep-ph\]](#).
- [32] A. Bochkarev, S. Kuzmin, and M. Shaposhnikov, “Electroweak baryogenesis and the Higgs boson mass problem,” [*Phys. Lett. B* **244** \(1990\) 275–278](#).

- [33] L. D. McLerran, M. E. Shaposhnikov, N. Turok, and M. B. Voloshin, “Why the baryon asymmetry of the universe is approximately 10^{10} ,” [Phys. Lett. B **256** \(1991\) 451–456](#).
- [34] A. Bochkarev, S. Kuzmin, and M. Shaposhnikov, “On the Model Dependence of the Cosmological Upper Bound on the Higgs Boson and Top Quark Masses,” [Phys. Rev. D **43** \(1991\) 369–374](#).
- [35] N. Turok and J. Zadrozny, “Electroweak baryogenesis in the two doublet model,” [Nucl. Phys. B **358** \(1991\) 471–493](#).
- [36] A. G. Cohen, D. Kaplan, and A. Nelson, “Spontaneous baryogenesis at the weak phase transition,” [Phys. Lett. B **263** \(1991\) 86–92](#).
- [37] N. Turok and J. Zadrozny, “Phase transitions in the two doublet model,” [Nucl. Phys. B **369** \(1992\) 729–742](#).
- [38] A. Nelson, D. Kaplan, and A. G. Cohen, “Why there is something rather than nothing: Matter from weak interactions,” [Nucl. Phys. B **373** \(1992\) 453–478](#).
- [39] K. Funakubo, A. Kakuto, and K. Takenaga, “The Effective potential of electroweak theory with two massless Higgs doublets at finite temperature,” [Prog. Theor. Phys. **91** \(1994\) 341–352](#), [arXiv:hep-ph/9310267](#).
- [40] A. Davies, C. Froggatt, G. Jenkins, and R. Moorhouse, “Baryogenesis constraints on two Higgs doublet models,” [Phys. Lett. B **336** \(1994\) 464–470](#).
- [41] K. Funakubo, A. Kakuto, S. Otsuki, K. Takenaga, and F. Toyoda, “CP violating profile of the electroweak bubble wall,” [Prog. Theor. Phys. **94** \(1995\) 845–860](#), [arXiv:hep-ph/9507452](#).
- [42] K. Funakubo, A. Kakuto, S. Otsuki, and F. Toyoda, “Explicit CP breaking and electroweak baryogenesis,” [Prog. Theor. Phys. **96** \(1996\) 771–780](#), [arXiv:hep-ph/9606282](#).
- [43] J. M. Cline, K. Kainulainen, and A. P. Vischer, “Dynamics of two Higgs doublet CP violation and baryogenesis at the electroweak phase transition,” [Phys. Rev. D **54** \(1996\) 2451–2472](#), [arXiv:hep-ph/9506284](#).
- [44] K. Fuyuto and E. Senaha, “Sphaleron and critical bubble in the scale invariant two Higgs doublet model,” [Phys. Lett. B **747** \(2015\) 152–157](#), [arXiv:1504.04291 \[hep-ph\]](#).
- [45] C.-W. Chiang, K. Fuyuto, and E. Senaha, “Electroweak Baryogenesis with Lepton Flavor Violation,” [Phys. Lett. B **762** \(2016\) 315–320](#), [arXiv:1607.07316 \[hep-ph\]](#).
- [46] G. Dorsch, S. Huber, and J. No, “A strong electroweak phase transition in the 2HDM after LHC8,” [JHEP **10** \(2013\) 029](#), [arXiv:1305.6610 \[hep-ph\]](#).
- [47] G. Dorsch, S. Huber, K. Mimasu, and J. No, “Echoes of the Electroweak Phase Transition: Discovering a second Higgs doublet through $A_0 \rightarrow ZH_0$,” [Phys. Rev. Lett. **113** \(2014\) no. 21, 211802](#), [arXiv:1405.5537 \[hep-ph\]](#).
- [48] J. M. Cline and P.-A. Lemieux, “Electroweak phase transition in two Higgs doublet models,” [Phys. Rev. D **55** \(1997\) 3873–3881](#), [arXiv:hep-ph/9609240](#).
- [49] L. Fromme, S. J. Huber, and M. Seniuch, “Baryogenesis in the two-Higgs doublet model,” [JHEP **11** \(2006\) 038](#), [arXiv:hep-ph/0605242](#).
- [50] J. M. Cline, K. Kainulainen, and M. Trott, “Electroweak Baryogenesis in Two Higgs Doublet Models and B meson anomalies,” [JHEP **11** \(2011\) 089](#), [arXiv:1107.3559 \[hep-ph\]](#).

- [51] G. Dorsch, S. Huber, T. Konstandin, and J. No, “A Second Higgs Doublet in the Early Universe: Baryogenesis and Gravitational Waves,” [*JCAP* **05** \(2017\) 052](#), [arXiv:1611.05874 \[hep-ph\]](#).
- [52] P. Basler, M. Krause, M. Muhlleitner, J. Wittbrodt, and A. Wlotzka, “Strong First Order Electroweak Phase Transition in the CP-Conserving 2HDM Revisited,” [*JHEP* **02** \(2017\) 121](#), [arXiv:1612.04086 \[hep-ph\]](#).
- [53] A. Haarr, A. Kvellestad, and T. C. Petersen, “Disfavouring Electroweak Baryogenesis and a hidden Higgs in a CP-violating Two-Higgs-Doublet Model,” [arXiv:1611.05757 \[hep-ph\]](#).
- [54] K. Fuyuto, W.-S. Hou, and E. Senaha, “Electroweak baryogenesis driven by extra top Yukawa couplings,” [*Phys. Lett. B* **776** \(2018\) 402–406](#), [arXiv:1705.05034 \[hep-ph\]](#).
- [55] G. Dorsch, S. Huber, K. Mimasu, and J. No, “The Higgs Vacuum Uplifted: Revisiting the Electroweak Phase Transition with a Second Higgs Doublet,” [*JHEP* **12** \(2017\) 086](#), [arXiv:1705.09186 \[hep-ph\]](#).
- [56] A. Cherchiglia and C. Nishi, “One-loop considerations for coexisting vacua in the CP conserving 2HDM,” [*JHEP* **11** \(2017\) 106](#), [arXiv:1707.04595 \[hep-ph\]](#).
- [57] P. Basler, M. Mühlleitner, and J. Wittbrodt, “The CP-Violating 2HDM in Light of a Strong First Order Electroweak Phase Transition and Implications for Higgs Pair Production,” [*JHEP* **03** \(2018\) 061](#), [arXiv:1711.04097 \[hep-ph\]](#).
- [58] J. O. Andersen, T. Gorda, A. Helset, L. Niemi, T. V. I. Tenkanen, A. Tranberg, A. Vuorinen, and D. J. Weir, “Nonperturbative Analysis of the Electroweak Phase Transition in the Two Higgs Doublet Model,” [*Phys. Rev. Lett.* **121** \(2018\) no. 19, 191802](#), [arXiv:1711.09849 \[hep-ph\]](#).
- [59] J. Bernon, L. Bian, and Y. Jiang, “A new insight into the phase transition in the early Universe with two Higgs doublets,” [*JHEP* **05** \(2018\) 151](#), [arXiv:1712.08430 \[hep-ph\]](#).
- [60] T. Gorda, A. Helset, L. Niemi, T. V. Tenkanen, and D. J. Weir, “Three-dimensional effective theories for the two Higgs doublet model at high temperature,” [*JHEP* **02** \(2019\) 081](#), [arXiv:1802.05056 \[hep-ph\]](#).
- [61] P. Basler and M. Mühlleitner, “BSMPT (Beyond the Standard Model Phase Transitions): A tool for the electroweak phase transition in extended Higgs sectors,” [*Comput. Phys. Commun.* **237** \(2019\) 62–85](#), [arXiv:1803.02846 \[hep-ph\]](#).
- [62] L. Wang, J. M. Yang, M. Zhang, and Y. Zhang, “Revisiting lepton-specific 2HDM in light of muon $g-2$ anomaly,” [*Phys. Lett. B* **788** \(2019\) 519–529](#), [arXiv:1809.05857 \[hep-ph\]](#).
- [63] K. Kainulainen, V. Keus, L. Niemi, K. Rummukainen, T. V. Tenkanen, and V. Vaskonen, “On the validity of perturbative studies of the electroweak phase transition in the Two Higgs Doublet model,” [*JHEP* **06** \(2019\) 075](#), [arXiv:1904.01329 \[hep-ph\]](#).
- [64] X. Wang, F. P. Huang, and X. Zhang, “Gravitational wave and collider signals in complex two-Higgs doublet model with dynamical CP-violation at finite temperature,” [*Phys. Rev. D* **101** \(2020\) no. 1, 015015](#), [arXiv:1909.02978 \[hep-ph\]](#).
- [65] D. Borah and J. M. Cline, “Inert Doublet Dark Matter with Strong Electroweak Phase Transition,” [*Phys. Rev. D* **86** \(2012\) 055001](#), [arXiv:1204.4722 \[hep-ph\]](#).

- [66] J. M. Cline and K. Kainulainen, “Improved Electroweak Phase Transition with Subdominant Inert Doublet Dark Matter,” [*Phys. Rev. D* **87** \(2013\) no. 7, 071701](#), [arXiv:1302.2614 \[hep-ph\]](#).
- [67] K. Fuyuto, J. Hisano, and E. Senaha, “Toward verification of electroweak baryogenesis by electric dipole moments,” [*Phys. Lett. B* **755** \(2016\) 491–497](#), [arXiv:1510.04485 \[hep-ph\]](#).
- [68] T. Modak and E. Senaha, “Electroweak baryogenesis via bottom transport,” [*Phys. Rev. D* **99** \(2019\) no. 11, 115022](#), [arXiv:1811.08088 \[hep-ph\]](#).
- [69] W. Chao and M. J. Ramsey-Musolf, “Catalysis of Electroweak Baryogenesis via Fermionic Higgs Portal Dark Matter,” [arXiv:1503.00028 \[hep-ph\]](#).
- [70] S. Inoue, G. Ovanessian, and M. J. Ramsey-Musolf, “Two-Step Electroweak Baryogenesis,” [*Phys. Rev. D* **93** \(2016\) 015013](#), [arXiv:1508.05404 \[hep-ph\]](#).
- [71] L. Niemi, H. H. Patel, M. J. Ramsey-Musolf, T. V. Tenkanen, and D. J. Weir, “Electroweak phase transition in the real triplet extension of the SM: Dimensional reduction,” [*Phys. Rev. D* **100** \(2019\) no. 3, 035002](#), [arXiv:1802.10500 \[hep-ph\]](#).
- [72] M. Chala, M. Ramos, and M. Spannowsky, “Gravitational wave and collider probes of a triplet Higgs sector with a low cutoff,” [*Eur. Phys. J. C* **79** \(2019\) no. 2, 156](#), [arXiv:1812.01901 \[hep-ph\]](#).
- [73] R. Zhou, W. Cheng, X. Deng, L. Bian, and Y. Wu, “Electroweak phase transition and Higgs phenomenology in the Georgi-Machacek model,” [*JHEP* **01** \(2019\) 216](#), [arXiv:1812.06217 \[hep-ph\]](#).
- [74] S. A. Ellis, S. Ipek, and G. White, “Electroweak Baryogenesis from Temperature-Varying Couplings,” [*JHEP* **08** \(2019\) 002](#), [arXiv:1905.11994 \[hep-ph\]](#).
- [75] Q.-H. Cao, F. P. Huang, K.-P. Xie, and X. Zhang, “Testing the electroweak phase transition in scalar extension models at lepton colliders,” [*Chin. Phys. C* **42** \(2018\) no. 2, 023103](#), [arXiv:1708.04737 \[hep-ph\]](#).
- [76] F. P. Huang, P.-H. Gu, P.-F. Yin, Z.-H. Yu, and X. Zhang, “Testing the electroweak phase transition and electroweak baryogenesis at the LHC and a circular electron-positron collider,” [*Phys. Rev. D* **93** \(2016\) no. 10, 103515](#), [arXiv:1511.03969 \[hep-ph\]](#).
- [77] F. P. Huang, Y. Wan, D.-G. Wang, Y.-F. Cai, and X. Zhang, “Hearing the echoes of electroweak baryogenesis with gravitational wave detectors,” [*Phys. Rev. D* **94** \(2016\) no. 4, 041702](#), [arXiv:1601.01640 \[hep-ph\]](#).
- [78] C. Balazs, G. White, and J. Yue, “Effective field theory, electric dipole moments and electroweak baryogenesis,” [*JHEP* **03** \(2017\) 030](#), [arXiv:1612.01270 \[hep-ph\]](#).
- [79] J. de Vries, M. Postma, J. van de Vis, and G. White, “Electroweak Baryogenesis and the Standard Model Effective Field Theory,” [*JHEP* **01** \(2018\) 089](#), [arXiv:1710.04061 \[hep-ph\]](#).
- [80] J. M. Cline, M. Jarvinen, and F. Sannino, “The Electroweak Phase Transition in Nearly Conformal Technicolor,” [*Phys. Rev. D* **78** \(2008\) 075027](#), [arXiv:0808.1512 \[hep-ph\]](#).
- [81] L. Bian, Y. Wu, and K.-P. Xie, “Electroweak phase transition with composite Higgs models: calculability, gravitational waves and collider searches,” [*JHEP* **12** \(2019\) 028](#), [arXiv:1909.02014 \[hep-ph\]](#).

- [82] K.-P. Xie, Y. Wu, and L. Bian, “Electroweak baryogenesis and gravitational waves in a composite Higgs model with high dimensional fermion representations,” [arXiv:2005.13552 \[hep-ph\]](#).
- [83] J. M. Cline, M. Joyce, and K. Kainulainen, “Supersymmetric electroweak baryogenesis in the WKB approximation,” [Phys. Lett. B](#) **417** (1998) 79–86, [arXiv:hep-ph/9708393](#). [Erratum: [Phys.Lett.B](#) 448, 321–321 (1999)].
- [84] A. Menon, D. Morrissey, and C. Wagner, “Electroweak baryogenesis and dark matter in the nMSSM,” [Phys. Rev. D](#) **70** (2004) 035005, [arXiv:hep-ph/0404184](#).
- [85] M. Carena, N. R. Shah, and C. E. Wagner, “Light Dark Matter and the Electroweak Phase Transition in the NMSSM,” [Phys. Rev. D](#) **85** (2012) 036003, [arXiv:1110.4378 \[hep-ph\]](#).
- [86] X.-J. Bi, L. Bian, W. Huang, J. Shu, and P.-F. Yin, “Interpretation of the Galactic Center excess and electroweak phase transition in the NMSSM,” [Phys. Rev. D](#) **92** (2015) 023507, [arXiv:1503.03749 \[hep-ph\]](#).
- [87] S. Demidov, D. Gorbunov, and D. Kirpichnikov, “Split NMSSM with electroweak baryogenesis,” [JHEP](#) **11** (2016) 148, [arXiv:1608.01985 \[hep-ph\]](#). [Erratum: [JHEP](#) 08, 080 (2017)].
- [88] W. Huang, Z. Kang, J. Shu, P. Wu, and J. M. Yang, “New insights in the electroweak phase transition in the NMSSM,” [Phys. Rev. D](#) **91** (2015) no. 2, 025006, [arXiv:1405.1152 \[hep-ph\]](#).
- [89] K. Cheung, T.-J. Hou, J. S. Lee, and E. Senaha, “Singlino-driven Electroweak Baryogenesis in the Next-to-MSSM,” [Phys. Lett. B](#) **710** (2012) 188–191, [arXiv:1201.3781 \[hep-ph\]](#).
- [90] C. Balázs, A. Mazumdar, E. Pukartas, and G. White, “Baryogenesis, dark matter and inflation in the Next-to-Minimal Supersymmetric Standard Model,” [JHEP](#) **01** (2014) 073, [arXiv:1309.5091 \[hep-ph\]](#).
- [91] S. J. Huber, T. Konstandin, T. Prokopec, and M. G. Schmidt, “Electroweak Phase Transition and Baryogenesis in the nMSSM,” [Nucl. Phys. B](#) **757** (2006) 172–196, [arXiv:hep-ph/0606298](#).
- [92] L. Bian, H.-K. Guo, and J. Shu, “Gravitational Waves, baryon asymmetry of the universe and electric dipole moment in the CP-violating NMSSM,” [Chin. Phys. C](#) **42** (2018) no. 9, 093106, [arXiv:1704.02488 \[hep-ph\]](#). [Erratum: [Chin.Phys.C](#) 43, 129101 (2019)].
- [93] J. Kozaczuk, S. Profumo, L. S. Haskins, and C. L. Wainwright, “Cosmological Phase Transitions and their Properties in the NMSSM,” [JHEP](#) **01** (2015) 144, [arXiv:1407.4134 \[hep-ph\]](#).
- [94] A. Katz, M. Perelstein, M. J. Ramsey-Musolf, and P. Winslow, “Stop-Catalyzed Baryogenesis Beyond the MSSM,” [Phys. Rev. D](#) **92** (2015) no. 9, 095019, [arXiv:1509.02934 \[hep-ph\]](#).
- [95] S. Akula, C. Balázs, L. Dunn, and G. White, “Electroweak baryogenesis in the \mathbb{Z}_3 -invariant NMSSM,” [JHEP](#) **11** (2017) 051, [arXiv:1706.09898 \[hep-ph\]](#).
- [96] C. Lee, V. Cirigliano, and M. J. Ramsey-Musolf, “Resonant relaxation in electroweak baryogenesis,” [Phys. Rev. D](#) **71** (2005) 075010, [arXiv:hep-ph/0412354](#).

- [97] C. Balazs, M. Carena, A. Menon, D. Morrissey, and C. Wagner, “The Supersymmetric origin of matter,” [*Phys. Rev. D* **71** \(2005\) 075002](#), [arXiv:hep-ph/0412264](#).
- [98] S. Liebler, S. Profumo, and T. Stefaniak, “Light Stop Mass Limits from Higgs Rate Measurements in the MSSM: Is MSSM Electroweak Baryogenesis Still Alive After All?,” [*JHEP* **04** \(2016\) 143](#), [arXiv:1512.09172 \[hep-ph\]](#).
- [99] A. Kobakhidze, L. Wu, and J. Yue, “Electroweak Baryogenesis with Anomalous Higgs Couplings,” [*JHEP* **04** \(2016\) 011](#), [arXiv:1512.08922 \[hep-ph\]](#).
- [100] M. J. Ramsey-Musolf, P. Winslow, and G. White, “Color Breaking Baryogenesis,” [*Phys. Rev. D* **97** \(2018\) no. 12, 123509](#), [arXiv:1708.07511 \[hep-ph\]](#).
- [101] S. Yaser Ayazi and A. Mohamadnejad, “Conformal vector dark matter and strongly first-order electroweak phase transition,” [*JHEP* **03** \(2019\) 181](#), [arXiv:1901.04168 \[hep-ph\]](#).
- [102] A. Mohamadnejad, “Gravitational waves from scale-invariant vector dark matter model: Probing below the neutrino-floor,” [*Eur. Phys. J. C* **80** \(2020\) no. 3, 197](#), [arXiv:1907.08899 \[hep-ph\]](#).
- [103] T. Lee, “A Theory of Spontaneous T Violation,” [*Phys. Rev. D* **8** \(1973\) 1226–1239](#).
- [104] G. C. Branco, P. M. Ferreira, L. Lavoura, M. N. Rebelo, M. Sher, and J. P. Silva, “Theory and phenomenology of two-Higgs-doublet models,” [*Phys. Rept.* **516** \(2012\) 1–102](#), [arXiv:1106.0034 \[hep-ph\]](#).
- [105] M. Fukugita and T. Yanagida, “Baryogenesis Without Grand Unification,” [*Phys. Lett. B* **174** \(1986\) 45–47](#).
- [106] I. Affleck and M. Dine, “A New Mechanism for Baryogenesis,” [*Nucl. Phys. B* **249** \(1985\) 361–380](#).
- [107] **FCC Collaboration**, A. Abada et al., “HE-LHC: The High-Energy Large Hadron Collider: Future Circular Collider Conceptual Design Report Volume 4,” [*Eur. Phys. J. ST* **228** \(2019\) no. 5, 1109–1382](#).
- [108] **CEPC Study Group Collaboration**, “CEPC Conceptual Design Report: Volume 2 - Physics & Detector,” [arXiv:1811.10545 \[hep-ex\]](#).
- [109] **CEPC Physics-Detector Study Group Collaboration**, “The CEPC input for the European Strategy for Particle Physics - Physics and Detector,” [arXiv:1901.03170 \[hep-ex\]](#).
- [110] S. Li, H. Song, and S. Su, “Probing Exotic Charged Higgs Decays in the Type-II 2HDM through Top Rich Signal at a Future 100 TeV pp Collider,” [arXiv:2005.00576 \[hep-ph\]](#).
- [111] F. Kling, H. Li, A. Pyarelal, H. Song, and S. Su, “Exotic Higgs Decays in Type-II 2HDMs at the LHC and Future 100 TeV Hadron Colliders,” [*JHEP* **06** \(2019\) 031](#), [arXiv:1812.01633 \[hep-ph\]](#).
- [112] C.-R. Chen, J. Hajer, T. Liu, I. Low, and H. Zhang, “Testing naturalness at 100 TeV,” [*JHEP* **09** \(2017\) 129](#), [arXiv:1705.07743 \[hep-ph\]](#).
- [113] N. Craig, J. Hajer, Y.-Y. Li, T. Liu, and H. Zhang, “Heavy Higgs bosons at low $\tan \beta$: from the LHC to 100 TeV,” [*JHEP* **01** \(2017\) 018](#), [arXiv:1605.08744 \[hep-ph\]](#).
- [114] P. Bambade et al., “The International Linear Collider: A Global Project,” [arXiv:1903.01629 \[hep-ex\]](#).

- [115] **FCC Collaboration**, A. Abada *et al.*, “FCC Physics Opportunities: Future Circular Collider Conceptual Design Report Volume 1,” [*Eur. Phys. J. C* **79** \(2019\) no. 6, 474](#).
- [116] **FCC Collaboration**, A. Abada *et al.*, “FCC-ee: The Lepton Collider: Future Circular Collider Conceptual Design Report Volume 2,” [*Eur. Phys. J. ST* **228** \(2019\) no. 2, 261–623](#).
- [117] **ATLAS Collaboration**, J. Lacey, “Higgs results from the combination of ATLAS and CMS,” <https://cds.cern.ch/record/2283082>.
- [118] J. Gu, H. Li, Z. Liu, S. Su, and W. Su, “Learning from Higgs Physics at Future Higgs Factories,” [*JHEP* **12** \(2017\) 153](#), [arXiv:1709.06103 \[hep-ph\]](#).
- [119] M. Laine and A. Vuorinen, [*Basics of Thermal Field Theory*](#), vol. 925. Springer, 2016. [arXiv:1701.01554 \[hep-ph\]](#).
- [120] S. R. Coleman and E. J. Weinberg, “Radiative Corrections as the Origin of Spontaneous Symmetry Breaking,” [*Phys. Rev. D* **7** \(1973\) 1888–1910](#).
- [121] M. Quiros, “Finite temperature field theory and phase transitions,” in [*ICTP Summer School in High-Energy Physics and Cosmology*](#), pp. 187–259. 1, 1999. [arXiv:hep-ph/9901312](#).
- [122] P. B. Arnold and O. Espinosa, “The Effective potential and first order phase transitions: Beyond leading-order,” [*Phys. Rev. D* **47** \(1993\) 3546](#), [arXiv:hep-ph/9212235](#). [Erratum: *Phys.Rev.D* 50, 6662 (1994)].
- [123] G. D. Moore, “Measuring the broken phase sphaleron rate nonperturbatively,” [*Phys. Rev. D* **59** \(1999\) 014503](#), [arXiv:hep-ph/9805264](#).
- [124] N. Nielsen, “On the Gauge Dependence of Spontaneous Symmetry Breaking in Gauge Theories,” [*Nucl. Phys. B* **101** \(1975\) 173–188](#).
- [125] L. Di Luzio and L. Mihaila, “On the gauge dependence of the Standard Model vacuum instability scale,” [*JHEP* **06** \(2014\) 079](#), [arXiv:1404.7450 \[hep-ph\]](#).
- [126] H. H. Patel and M. J. Ramsey-Musolf, “Baryon Washout, Electroweak Phase Transition, and Perturbation Theory,” [*JHEP* **07** \(2011\) 029](#), [arXiv:1101.4665 \[hep-ph\]](#).
- [127] M. Laine, M. Meyer, and G. Nardini, “Thermal phase transition with full 2-loop effective potential,” [*Nucl. Phys. B* **920** \(2017\) 565–600](#), [arXiv:1702.07479 \[hep-ph\]](#).
- [128] M. Dine, P. Huet, and J. Singleton, Robert L., “Baryogenesis at the electroweak scale,” [*Nucl. Phys. B* **375** \(1992\) 625–648](#).
- [129] C. L. Wainwright, “CosmoTransitions: Computing Cosmological Phase Transition Temperatures and Bubble Profiles with Multiple Fields,” [*Comput. Phys. Commun.* **183** \(2012\) 2006–2013](#), [arXiv:1109.4189 \[hep-ph\]](#).
- [130] P. Athron, C. Balázs, A. Fowlie, and Y. Zhang, “PhaseTracer: tracing cosmological phases and calculating transition properties,” [*Eur. Phys. J. C* **80** \(2020\) no. 6, 567](#), [arXiv:2003.02859 \[hep-ph\]](#).
- [131] T. Han, S. K. Kang, and J. Sayre, “Muon $g - 2$ in the aligned two Higgs doublet model,” [*JHEP* **02** \(2016\) 097](#), [arXiv:1511.05162 \[hep-ph\]](#).
- [132] F. Kling, S. Su, and W. Su, “2HDM Neutral Scalars under the LHC,” [*JHEP* **06** \(2020\) 163](#), [arXiv:2004.04172 \[hep-ph\]](#).

- [133] N. G. Deshpande and E. Ma, “Pattern of Symmetry Breaking with Two Higgs Doublets,” [*Phys. Rev. D* **18** \(1978\) 2574](#).
- [134] M. Sher, “Electroweak Higgs Potentials and Vacuum Stability,” [*Phys. Rept.* **179** \(1989\) 273–418](#).
- [135] S. Nie and M. Sher, “Vacuum stability bounds in the two Higgs doublet model,” [*Phys. Lett. B* **449** \(1999\) 89–92](#), [arXiv:hep-ph/9811234](#).
- [136] S. Kanemura, T. Kasai, and Y. Okada, “Mass bounds of the lightest CP even Higgs boson in the two Higgs doublet model,” [*Phys. Lett. B* **471** \(1999\) 182–190](#), [arXiv:hep-ph/9903289](#).
- [137] H. Hufel and G. Pocsik, “Unitarity Bounds on Higgs Boson Masses in the Weinberg-Salam Model With Two Higgs Doublets,” [*Z. Phys. C* **8** \(1981\) 13](#).
- [138] J. Maalampi, J. Sirkka, and I. Vilja, “Tree level unitarity and triviality bounds for two Higgs models,” [*Phys. Lett. B* **265** \(1991\) 371–376](#).
- [139] S. Kanemura, T. Kubota, and E. Takasugi, “Lee-Quigg-Thacker bounds for Higgs boson masses in a two doublet model,” [*Phys. Lett. B* **313** \(1993\) 155–160](#), [arXiv:hep-ph/9303263](#).
- [140] A. G. Akeroyd, A. Arhrib, and E.-M. Naimi, “Note on tree level unitarity in the general two Higgs doublet model,” [*Phys. Lett. B* **490** \(2000\) 119–124](#), [arXiv:hep-ph/0006035](#).
- [141] I. Ginzburg and I. Ivanov, “Tree-level unitarity constraints in the most general 2HDM,” [*Phys. Rev. D* **72** \(2005\) 115010](#), [arXiv:hep-ph/0508020](#).
- [142] W. Su, “Probing loop effects in wrong-sign Yukawa region of 2HDM,” [arXiv:1910.06269 \[hep-ph\]](#).
- [143] **CMS** Collaboration, A. M. Sirunyan et al., “Search for MSSM Higgs bosons decaying to $\mu^+\mu^-$ in proton-proton collisions at $\sqrt{s} = 13$ TeV Search for MSSM Higgs bosons decaying to $\mu^+\mu^-$ in proton-proton collisions at $\sqrt{s} = 13$ TeV,” [*Phys. Lett. B* **798** \(2019\) 134992](#), [arXiv:1907.03152 \[hep-ex\]](#).
- [144] **ATLAS** Collaboration, M. Aaboud et al., “Search for scalar resonances decaying into $\mu^+\mu^-$ in events with and without b -tagged jets produced in proton-proton collisions at $\sqrt{s} = 13$ TeV with the ATLAS detector,” [*JHEP* **07** \(2019\) 117](#), [arXiv:1901.08144 \[hep-ex\]](#).
- [145] **CMS** Collaboration, A. M. Sirunyan et al., “Search for beyond the standard model Higgs bosons decaying into a $b\bar{b}$ pair in pp collisions at $\sqrt{s} = 13$ TeV,” [*JHEP* **08** \(2018\) 113](#), [arXiv:1805.12191 \[hep-ex\]](#).
- [146] **ATLAS** Collaboration, G. Aad et al., “Search for heavy neutral Higgs bosons produced in association with b -quarks and decaying to b -quarks at $\sqrt{s} = 13$ TeV with the ATLAS detector,” [arXiv:1907.02749 \[hep-ex\]](#).
- [147] **CMS** Collaboration, A. M. Sirunyan et al., “Search for additional neutral MSSM Higgs bosons in the $\tau\tau$ final state in proton-proton collisions at $\sqrt{s} = 13$ TeV,” [*JHEP* **09** \(2018\) 007](#), [arXiv:1803.06553 \[hep-ex\]](#).
- [148] **CMS** Collaboration, A. M. Sirunyan et al., “Search for a low-mass $\tau^+\tau^-$ resonance in association with a bottom quark in proton-proton collisions at $\sqrt{s} = 13$ TeV,” [*JHEP* **05** \(2019\) 210](#), [arXiv:1903.10228 \[hep-ex\]](#).

- [149] **ATLAS** Collaboration, G. Aad *et al.*, “Search for heavy Higgs bosons decaying into two tau leptons with the ATLAS detector using pp collisions at $\sqrt{s} = 13$ TeV,” [arXiv:2002.12223 \[hep-ex\]](#).
- [150] **CMS** Collaboration, A. M. Sirunyan *et al.*, “Search for a standard model-like Higgs boson in the mass range between 70 and 110 GeV in the diphoton final state in proton-proton collisions at $\sqrt{s} = 8$ and 13 TeV,” [Phys. Lett. B793 \(2019\) 320–347](#), [arXiv:1811.08459 \[hep-ex\]](#).
- [151] **CMS** Collaboration, A. M. Sirunyan *et al.*, “Search for physics beyond the standard model in high-mass diphoton events from proton-proton collisions at $\sqrt{s} = 13$ TeV,” [Phys. Rev. D98 \(2018\) no. 9, 092001](#), [arXiv:1809.00327 \[hep-ex\]](#).
- [152] **ATLAS** Collaboration, G. Aad *et al.*, “Search for Scalar Diphoton Resonances in the Mass Range 65 – 600 GeV with the ATLAS Detector in pp Collision Data at $\sqrt{s} = 8$ TeV,” [Phys. Rev. Lett. 113 \(2014\) no. 17, 171801](#), [arXiv:1407.6583 \[hep-ex\]](#).
- [153] **ATLAS** Collaboration, M. Aaboud *et al.*, “Search for new phenomena in high-mass diphoton final states using 37 fb⁻¹ of proton-proton collisions collected at $\sqrt{s} = 13$ TeV with the ATLAS detector,” [Phys. Lett. B775 \(2017\) 105–125](#), [arXiv:1707.04147 \[hep-ex\]](#).
- [154] **ATLAS** Collaboration, T. A. collaboration, “Search for resonances in the 65 to 110 GeV diphoton invariant mass range using 80 fb⁻¹ of pp collisions collected at $\sqrt{s} = 13$ TeV with the ATLAS detector,”.
- [155] **CMS** Collaboration, A. M. Sirunyan *et al.*, “Search for heavy Higgs bosons decaying to a top quark pair in proton-proton collisions at $\sqrt{s} = 13$ TeV,” [arXiv:1908.01115 \[hep-ex\]](#).
- [156] **CMS** Collaboration, A. M. Sirunyan *et al.*, “Search for a new scalar resonance decaying to a pair of Z bosons in proton-proton collisions at $\sqrt{s} = 13$ TeV,” [JHEP 06 \(2018\) 127](#), [arXiv:1804.01939 \[hep-ex\]](#). [Erratum: JHEP03,128(2019)].
- [157] **ATLAS** Collaboration, M. Aaboud *et al.*, “Search for heavy ZZ resonances in the $\ell^+\ell^-\ell^+\ell^-$ and $\ell^+\ell^-\nu\bar{\nu}$ final states using proton-proton collisions at $\sqrt{s} = 13$ TeV with the ATLAS detector,” [Eur. Phys. J. C78 \(2018\) no. 4, 293](#), [arXiv:1712.06386 \[hep-ex\]](#).
- [158] **CMS** Collaboration, A. M. Sirunyan *et al.*, “Search for a heavy Higgs boson decaying to a pair of W bosons in proton-proton collisions at $\sqrt{s} = 13$ TeV,” [arXiv:1912.01594 \[hep-ex\]](#).
- [159] **ATLAS** Collaboration, M. Aaboud *et al.*, “Search for heavy resonances decaying into WW in the $e\nu\mu\nu$ final state in pp collisions at $\sqrt{s} = 13$ TeV with the ATLAS detector,” [Eur. Phys. J. C78 \(2018\) no. 1, 24](#), [arXiv:1710.01123 \[hep-ex\]](#).
- [160] **CMS** Collaboration, V. Khachatryan *et al.*, “Search for a pseudoscalar boson decaying into a Z boson and the 125 GeV Higgs boson in $l\bar{l}b\bar{b}$ final states,” [Phys. Lett. B748 \(2015\) 221–243](#), [arXiv:1504.04710 \[hep-ex\]](#).
- [161] **CMS** Collaboration, A. M. Sirunyan *et al.*, “Search for a heavy pseudoscalar boson decaying to a Z and a Higgs boson at $\sqrt{s} = 13$ TeV,” [Eur. Phys. J. C79 \(2019\) no. 7, 564](#), [arXiv:1903.00941 \[hep-ex\]](#).
- [162] **ATLAS** Collaboration, G. Aad *et al.*, “Search for a CP-odd Higgs boson decaying to Zh in pp collisions at $\sqrt{s} = 8$ TeV with the ATLAS detector,” [Phys. Lett. B744 \(2015\) 163–183](#), [arXiv:1502.04478 \[hep-ex\]](#).

- [163] **ATLAS** Collaboration, M. Aaboud *et al.*, “Search for heavy resonances decaying into a W or Z boson and a Higgs boson in final states with leptons and b -jets in 36 fb^{-1} of $\sqrt{s} = 13\text{ TeV}$ pp collisions with the ATLAS detector,” [*JHEP* **03** \(2018\) 174](#), [arXiv:1712.06518 \[hep-ex\]](#). [Erratum: *JHEP*11,051(2018)].
- [164] **CMS** Collaboration, V. Khachatryan *et al.*, “Searches for a heavy scalar boson H decaying to a pair of 125 GeV Higgs bosons hh or for a heavy pseudoscalar boson A decaying to Zh , in the final states with $h \rightarrow \tau\tau$,” [*Phys. Lett.* **B755** \(2016\) 217–244](#), [arXiv:1510.01181 \[hep-ex\]](#).
- [165] **CMS** Collaboration, A. M. Sirunyan *et al.*, “Search for a heavy pseudoscalar Higgs boson decaying into a 125 GeV Higgs boson and a Z boson in final states with two tau and two light leptons at $\sqrt{s} = 13\text{ TeV}$,” [arXiv:1910.11634 \[hep-ex\]](#).
- [166] **CMS** Collaboration, A. M. Sirunyan *et al.*, “Search for Higgs boson pair production in the $bb\tau\tau$ final state in proton-proton collisions at $\sqrt{s} = 8\text{ TeV}$,” [*Phys. Rev.* **D96** \(2017\) no. 7, 072004](#), [arXiv:1707.00350 \[hep-ex\]](#).
- [167] **CMS** Collaboration, A. M. Sirunyan *et al.*, “Combination of searches for Higgs boson pair production in proton-proton collisions at $\sqrt{s} = 13\text{ TeV}$,” [*Phys. Rev. Lett.* **122** \(2019\) no. 12, 121803](#), [arXiv:1811.09689 \[hep-ex\]](#).
- [168] **ATLAS** Collaboration, G. Aad *et al.*, “Searches for Higgs boson pair production in the $hh \rightarrow bb\tau\tau, \gamma\gamma WW^*, \gamma\gamma bb, bbbb$ channels with the ATLAS detector,” [*Phys. Rev.* **D92** \(2015\) 092004](#), [arXiv:1509.04670 \[hep-ex\]](#).
- [169] **ATLAS** Collaboration, G. Aad *et al.*, “Combination of searches for Higgs boson pairs in pp collisions at $\sqrt{s} = 13\text{ TeV}$ with the ATLAS detector,” [arXiv:1906.02025 \[hep-ex\]](#).
- [170] **ATLAS** Collaboration, M. Aaboud *et al.*, “Search for a heavy Higgs boson decaying into a Z boson and another heavy Higgs boson in the $\ell\ell bb$ final state in pp collisions at $\sqrt{s} = 13\text{ TeV}$ with the ATLAS detector,” [*Phys. Lett.* **B783** \(2018\) 392–414](#), [arXiv:1804.01126 \[hep-ex\]](#).
- [171] **CMS** Collaboration, A. M. Sirunyan *et al.*, “Search for new neutral Higgs bosons through the $H \rightarrow ZA \rightarrow \ell^+\ell^- b\bar{b}$ process in pp collisions at $\sqrt{s} = 13\text{ TeV}$,” [arXiv:1911.03781 \[hep-ex\]](#).
- [172] S. Liebler, S. Patel, and G. Weiglein, “Phenomenology of on-shell Higgs production in the MSSM with complex parameters,” [*Eur. Phys. J.* **C77** \(2017\) no. 5, 305](#), [arXiv:1611.09308 \[hep-ph\]](#).
- [173] D. Eriksson, J. Rathsmann, and O. Stal, “2HDMC: Two-Higgs-Doublet Model Calculator Physics and Manual,” [*Comput. Phys. Commun.* **181** \(2010\) 189–205](#), [arXiv:0902.0851 \[hep-ph\]](#).
- [174] W. Su, M. White, A. G. Williams, and Y. Wu, “Exploring the low $\tan\beta$ region of two Higgs doublet models at the LHC,” [arXiv:1909.09035 \[hep-ph\]](#).
- [175] **ALEPH, DELPHI, L3, OPAL, SLD, LEP Electroweak Working Group, SLD Electroweak Group, SLD Heavy Flavour Group** Collaboration, S. Schael *et al.*, “Precision electroweak measurements on the Z resonance,” [*Phys. Rept.* **427** \(2006\) 257–454](#), [arXiv:hep-ex/0509008 \[hep-ex\]](#).
- [176] J. Haller, A. Hoecker, R. Kogler, K. Mönig, T. Peiffer, and J. Stelzer, “Update of the global electroweak fit and constraints on two-Higgs-doublet models,” [*Eur. Phys. J.* **C78** \(2018\) no. 8, 675](#), [arXiv:1803.01853 \[hep-ph\]](#).

- [177] N. Chen, T. Han, S. Li, S. Su, W. Su, and Y. Wu, “Type-I 2HDM under the Higgs and Electroweak Precision Measurements,” [arXiv:1912.01431 \[hep-ph\]](#).
- [178] N. Chen, T. Han, S. Su, W. Su, and Y. Wu, “Type-II 2HDM under the Precision Measurements at the Z -pole and a Higgs Factory,” [JHEP 03 \(2019\) 023](#), [arXiv:1808.02037 \[hep-ph\]](#).
- [179] **HFLAV** Collaboration, Y. Amhis *et al.*, “Averages of b -hadron, c -hadron, and τ -lepton properties as of summer 2016,” [Eur. Phys. J. C77 \(2017\) no. 12, 895](#), [arXiv:1612.07233 \[hep-ex\]](#).
- [180] A. Arbey, F. Mahmoudi, O. Stal, and T. Stefaniak, “Status of the Charged Higgs Boson in Two Higgs Doublet Models,” [Eur. Phys. J. C 78 \(2018\) no. 3, 182](#), [arXiv:1706.07414 \[hep-ph\]](#).